

709



Department of Energy  
Washington, DC 20585

OCT 5 1992

Mr. Joseph J. Holonich, Director  
Repository Licensing & Quality Assurance  
Project Directorate  
Division of High-Level Waste Management  
Office of Nuclear Material Safety  
and Safeguards  
U.S. Nuclear Regulatory Commission  
Washington, D.C. 20555

Dear Mr. Holonich:

In its Phase I review of the U.S. Department of Energy's (DOE) Study Plan 8.3.1.2.2.3, "Characterization of the Percolation in the Unsaturated Zone-Surface-Based Study," the U.S. Nuclear Regulatory Commission (NRC) requested that DOE provide references cited in the study plan that are not readily available in the public domain (enclosure 1). Enclosure 2 contains the references requested for Study Plan 8.3.1.2.2.3.

If you have any questions, please contact Mr. Chris Einberg of my office at 202-586-8869.

Sincerely,

John P. Roberts  
Acting Associate Director for  
Systems and Compliance  
Office of Civilian Radioactive  
Waste Management

Enclosures:

- 1. Ltr, 3/26/92, Holonich to Roberts,  
w/encl
- 2. References for Study  
Plan 8.3.1.2.2.3  
(Not Record Material)

*on the shelf*

160072

9212170132 921005  
PDR WASTE PDR  
WM-11

ADD: Charlotte Abrams

Chr. Encl.  
| |

102.8  
WM-11 1/1  
NH03

cc: w\enclosures  
Alice Cortinas, CNWRA, San Antonio, TX

cc: w\enclosures  
C. Gertz, YMPO  
R. Loux, State of Nevada  
T. Hickey, Nevada Legislative Commission  
M. Baughman, Lincoln County, NV  
J. Bingham, Clark County, NV  
B. Raper, Nye County, NV  
P. Niedzielski-Eichner, Nye County, NV  
G. Derby, Lander County, NV  
P. Goicoechea, Eureka, NV  
C. Schank, Churchill County, NV  
F. Mariani, White Pine County, NV  
V. Poe, Mineral County, NV  
E. Wright, Lincoln County, NV  
J. Pitts, Lincoln County, NV  
R. Williams, Lander County, NV  
J. Hayes, Esmeralda County, NV  
M. Hayes, Esmeralda County, NV  
B. Mettam, Inyo County, CA  
C. Abrams, NRC



UNITED STATES  
NUCLEAR REGULATORY COMMISSION  
WASHINGTON, D. C. 20555

MAR 26 1992

Mr. John P. Roberts, Acting Associate Director  
for Systems and Compliance  
Office of Civilian Radioactive Waste Management  
U.S. Department of Energy  
Washington, DC 20585

Dear Mr. Roberts:

SUBJECT: PHASE I REVIEW OF U.S. DEPARTMENT OF ENERGY (DOE) STUDY PLAN FOR CHARACTERIZATION OF THE PERCOLATION IN THE UNSATURATED-ZONE - SURFACE-BASED STUDY

On May 10, 1991, DOE transmitted the study plan, "Characterization of the Percolation in the Unsaturated Zone - Surface-Based Study" (Study Plan 8.3.1.2.2.3) to the U.S. Nuclear Regulatory Commission (NRC) for review and comment. NRC has completed its Phase I Review of this document using the Review Plan for NRC Staff Review of DOE Study Plans, Revision 1 (December 6, 1990).

The material submitted in the study plan was considered to be consistent, to the extent possible at this time, with the NRC-DOE agreement on content of study plans made at the May 7-8, 1986, meeting on Level of Detail for Site Characterization Plans and Study Plans. The NRC staff recognizes that some of the information required in the agreement, especially many of the technical procedures for field and laboratory tests, cannot be provided until the prototype testing described in the study plan is completed. The staff did not consider that the absence of such information compromised its ability to conduct its Phase I Review of the material provided. However, the NRC staff requests that the procedures, methods, and other relevant details be provided to NRC for its review as soon as that information is available.

Among the references listed for this study plan are several which have not been provided to NRC and are not readily available in the public domain. We therefore request that DOE provide the NRC with the documents which are listed in the Enclosure.

A major purpose of the Phase I Review is to identify concerns with studies, tests, or analyses that, if started, could cause significant and irreparable adverse effects on the site, the site characterization program, or the eventual usability of the data for licensing. Such concerns would constitute objections, as that term has been used in earlier NRC staff reviews of DOE's documents related to site characterization (Consultation Draft Site Characterization Plan and the Site Characterization Plan for the Yucca Mountain site).

It does not appear that the conduct of the activities described in this study plan will have significant adverse impacts on repository performance and the Phase I Review of this study plan identified no objections with any of the

9204010076 #318

ENCLOSURE 1

activities proposed. This decision was influenced by the following considerations: 1) the information from this study plan is important to site characterization; 2) there does not appear to be a noninvasive method of collecting the data; 3) the study plan commits to sealing each unsaturated zone borehole within the Conceptual Perimeter Drift Boundary; and 4) the study plan has outlined a process to develop acceptable borehole sealing requirements and approaches. The NRC staff expects that proper sealing of boreholes will be performed consistent with 10 CFR 60.134 (a) which states, "Seals for shafts and boreholes shall be designed so that following permanent closure they do not become pathways that compromise the geologic repository's ability to meet the performance objectives for the period following permanent closure." These conclusions regarding boreholes described in this study plan should not be construed to mean that the NRC has reached the same conclusions with respect to additional or other boreholes not identified in this study plan (i.e., study plan 8.3.1.2.2.3, Revision 0).

After completion of the Phase I Review, selected study plans are to receive a second level of review, called a Detailed Technical Review, based on the relationship of a given study plan to key site-specific issues or NRC open items, or its reliance on unique, state-of-the-art test or analysis methods. We have decided not to proceed with a Detailed Technical Review of this study plan at this time, in part because the technical details required for such a review will not be available until the prototype studies are completed.

If you have any questions concerning this letter, please contact Charlotte Abrams (301)504-3403/FTS964-3403 of my staff.

Sincerely,



Joseph J. Holonich, Director  
Repository Licensing and Quality  
Assurance Project Directorate  
Division of High-Level Waste Management  
Office of Nuclear Material Safety  
and Safeguards

Enclosure: As stated

cc: R. Loux, State of Nevada  
C. Gertz, DOE/NV  
S. Bradhurst, Nye County, NV  
M. Baughman, Lincoln County, NV  
D. Bechtel, Clark County, NV  
D. Weigel, GAO  
P. Niedzielski-Eichner, Nye County, NV  
C. Thistlethwaite, Inyo County, CA  
V. Poe, Mineral County, NV  
F. Sperry, White Pine County, NV  
R. Williams, Lander County, NV  
P. Goicoechea, Eureka County, NV  
L. Vaughan II, Esmeralda County, NV  
C. Shank, Churchill County, NV  
T. J. Hickey, Nevada Legislative Committee

References for Study Plan 8.3.1.2.2.3  
Requested by NRC

- ✓ Agarwal, R. G., 1979, Real gas pseudotime - a new function for pressure buildup analysis of MHF gas wells: Paper SPE 8279 presented at the 1979 SPE Annual Technical Conference and Exhibition, Las Vegas, Nevada, September 23-26.
- ✓ Cunningham, D. A., 1988, Computer and physical VSP modeling of Yucca Mountain, Nevada: Master of Science Thesis #T-3637, Colorado School of Mines, Golden, Colorado.
- Copyright in this system not distributed*  
✓ Stenseth, J. P., and Gaiser, S. E., 1983, Three-component vertical seismic profiles, an application of Gal'perin's polarization position correlation technique: 53rd Annual SEG Extended Abstracts, Los Angeles. \*
- ✓ Flint, A. L., and Flint, L. E., in progress, Preliminary permeability and water retention data for nonwelded and bedded tuff samples, Yucca Mountain area, Nye County, Nevada: U.S. Geological Survey Open-File Report 90-XXX.
- ✓ Gal'perin, 1980, Results of using the polarization method of vertical seismic profiling in the territory of Krasnodar Region: Express Informatzia, Ministry of Geology, Moscow, no. 16, p. 27.
- ..... 1984, The polarization method of seismic exploration: Boston, D. Reidel Publishing Co., Esp. Chapter 5, "Polarization Position Correlation (PPC) of Seismic Waves, pp. 158-202, (trans. from the Russian, Nedro Moscow), 268 p. \*
- ✓ Karus, E. V., and others, 1975, Detailed investigation of geologic structures by seismic well surveys: Ninth World Petroleum Congress PD, 9(4), v. 25, p. 247.
- ✓ Montazer, P. and Wilson, W. E., 1985, Hydrogeology of the unsaturated zone, Yucca Mountain, Nevada, in NWA Conference on Characterization and Monitoring of the Vadose (Unsaturated) Zone, Proceedings: Dublin, Ohio, National Water Well Association, p. 396-412.
- ✓ Skuse, B., 1984, Capillary pressure measurement in reservoir rock cores using the centrifuge: Applications Data, Beckman Institute, Inc., Palo Alto, California, 4 p.
- ✓ Snow, D. T., January 1965, A parallel plate model of fractured permeable media: Ph.D. dissertation, University of California, Berkeley, California. \*
- ✓ ..... 1966, Three-hole pressure tests for anisotropic foundation permeability: Fels. U. Ing. Geology, v. 4, p. 298.

\* Copyright material, not submitted to DCC

*rec'd with letter dtd  
10/5/92*

U.S. DEPARTMENT OF ENERGY

**YUCCA  
MOUNTAIN**



**YUCCA MOUNTAIN  
SITE CHARACTERIZATION  
PROJECT**

**REFERENCES  
FOR  
STUDY PLAN 8.3.1.2.2.3**



*102.8*

**ENCLOSURE 2**

SPE 8279

## "REAL GAS PSEUDO-TIME" - A NEW FUNCTION FOR PRESSURE BUILDUP ANALYSIS OF MHF GAS WELLS

by Ram G. Agarwal, Member SPE-AIME,  
Amoco Production Co.

© Copyright 1979, American Institute of Mining, Metallurgical, and Petroleum Engineers, Inc.

This paper was presented at the 56th Annual Fall Technical Conference and Exhibition of the Society of Petroleum Engineers of AIME, held at Las Vegas, Nevada, September 23-28, 1979. The material is subject to revision by the author. Permission to copy is granted in an abstract of not more than 200 words. Write SPE at Central Dept., Dallas, Texas 75201.

### ABSTRACT

A new time function has been defined which considers variations of gas viscosity and compressibility as a function of pressure, which in turn is a function of time. This function appears to be similar to the real gas pseudo-pressure,  $m(p)$ , of Al-Hussainy et al., which takes into account the variations of gas viscosity and z-factor as a function of pressure. However, this is an approximate function as opposed to  $m(p)$ . This time function will be referred to in this paper as the real gas pseudo-time,  $t(p)$ . This function has aided in post-treatment pressure buildup analysis of fractured (including MHF) gas wells by type curve analysis. Results of computer simulated pressure buildup analysis indicate that the use of  $t(p)$  provides satisfactory values of computed fracture lengths in fractured gas wells.

In this paper the real gas pseudo-time is described and its application is demonstrated by means of example problems. Although the discussion in this paper is limited to pressure buildup analysis of vertically fractured gas wells, the utility of this function is not meant to be restricted to such wells only.

### INTRODUCTION

In recent years, type curve analysis methods<sup>1</sup> have become well known in the petroleum industry for analyzing both pressure drawdown and buildup data in oil and gas wells. These methods are meant to be used in conjunction with the conventional methods whenever possible. Exceptions appear to be MHF gas wells with finite flow capacity fractures where conventional methods are not readily applicable and, at least to date, only type curve methods appear practical to determine fracture length and fracture flow capacity. Although the majority of published type curves,<sup>1</sup> including those for MHF wells,<sup>2,3</sup> are based on the pressure drawdown solutions for liquid systems, they can be used in an approximate fashion to analyze pressure data from real gas wells. The first requirement is that the dimensionless pressure

References and illustrations at end of paper.

and time variables are appropriately defined for gas wells. For example, to use the liquid system type curves for an MHF gas well, dimensionless variables are defined as follows:<sup>2</sup>

Dimensionless pressure,

$$P_{wD} = \frac{kh \Delta(m(p))}{1424 qI} \quad (1)$$

(In SI units, the numerical constant is  $1.28 \times 10^{-3}$ )

Dimensionless pressure, for a gas well, may also be expressed in terms of  $\Delta(p^2)$  or  $\Delta p$ .

Dimensionless time,

$$t_{Dx_f} = \frac{2.634 \times 10^{-6} kt}{\phi(\mu c_t)_i x_f^2} \quad (2)$$

(In SI units, the numerical constant is  $3.6 \times 10^{-9}$ )

The definition of dimensionless fracture capacity remains the same.

$$F_{CD} = \frac{k_f v}{kr_f} \quad (3)$$

Note that in Eq. (1), the real gas pseudo-pressure,  $m(p)$  of Al-Hussainy et al.<sup>4,5</sup> has been used to take into account the variations of gas viscosity and z-factor as a function of pressure. In Eq. (2), viscosity-compressibility  $(\mu c_t)_i$  is shown to be evaluated at the initial reservoir pressure.

In analyzing pressure drawdown data from real gas wells using a liquid system type curve, it is recommended that the real gas pseudo-pressure is

8.3.1.223  
Encl. 2

used and  $\Delta[m(p)]$  to be used in Eq. (1) is defined as follows:

$$\Delta[m(p)] = m(p_i) - m(p_{wf}) \quad (4)$$

It has been also established that in analyzing pressure drawdown data from gas wells by type curve matching, reasonable answers are obtained if the  $(\mu c_p)$  product in Eq. 2 is evaluated at the initial reservoir pressure.<sup>4</sup>

In analyzing pressure buildup data using drawdown type curves, the additional restriction which should be imposed is that the producing time,  $t_p$  prior to shut-in is significantly greater than  $t_p$  the shut-in time,  $\Delta t$  that is  $(t_p + \Delta t)/\Delta t \approx 1$ . This should apply to both oil and gas wells. In the case of gas well buildup analysis,  $\Delta[m(p)]$  is defined as follows:

$$\Delta[m(p)] = m(p_{\Delta t}) - m(p_{\Delta t=0}) \quad (5)$$

However, in using type curves for analyzing pressure buildup data especially from fractured gas wells (even if the effect of producing time is insignificant), it is not clear as to which pressure level the  $(\mu c_p)$  product in the dimensionless term should be evaluated. The question arises whether the  $(\mu c_p)$  product should be evaluated at (1) the initial reservoir pressure, (2) the final flowing pressure prior to shut-in, or (3) some average pressure. Results of this study indicate that the use of any one of the above three pressure levels is less than satisfactory. In general, the use of the initial reservoir pressure resulted in a fracture length value greater than the actual; the use of the final flowing pressure provided a computed fracture length which was smaller than the actual; and the use of an average pressure provided a fracture length value which was different than that used in the computer model.

To overcome the above difficulty, a new time function has been studied. This has aided us in post-treatment pressure buildup analysis of fractured (including MHF) gas wells. This function considers variations of gas viscosity and compressibility as a function of pressure, which in turn is a function of time. This function is named real gas pseudo-time,  $t(p)$ , in this paper. This function is analogous to the real gas pseudo-pressure,  $m(p)$  of Al-Hussainy et al.,<sup>4,6</sup> which includes the effects of pressure dependent gas viscosity and z-factor. It should be emphasized that  $t(p)$  is an approximate function as opposed to  $m(p)$ . However, it provides reasonable values of fracture lengths in pressure buildup analysis of vertically fractured gas wells and should be most useful for MHF gas wells.

The discussion in this paper will deal with the applicability and limitations of liquid system drawdown type curves in analyzing pressure buildup data from gas wells. However, type curves for only vertically fractured wells will be considered.

The discussion will also include a description of the new time function, its computational procedure and application by means of example problems.

## TYPE CURVES FOR VERTICALLY FRACTURED WELLS

During the past few years, type curves have appeared in the petroleum literature which can be used to analyze pressure data from vertically fractured wells. Gringarten et al.<sup>6</sup> presented type curves for infinite flow capacity fractures. Since their type curves could not be used for MHF wells with finite capacity fractures, Cinco et al.<sup>3</sup> and Agarwal et al.<sup>2</sup> published new sets of type curves (finite fracture flow capacity) for MHF wells. Constant wellbore rate type curves of Gringarten et al.<sup>6</sup> and Agarwal et al.<sup>2</sup> are shown in Figs. 1 and 2, respectively. Since all these type curves are based on the pressure drawdown data in liquid systems, it may first appear that they may not be used to analyze (1) pressure buildup data in oil wells, and (2) pressure drawdown and buildup data in gas wells. Results of this study indicate that the above type curves can be used, at least in an approximate fashion, to analyze a variety of drawdown and buildup problems provided certain restrictions are realized and a few modifications are made. These restrictions will be examined next.

### 1. Use of Drawdown Type Curves for Buildup

Let us first examine the validity and limitations of liquid system drawdown type curves (see Figs. 1 and 2) to analyze pressure buildup data in oil wells. Before these type curves may be used, it is important to note the duration of producing time,  $t_p$  compared to shut-in time,  $\Delta t$ .

#### a) Small producing time

If the producing time,  $t_p$  prior to shut-in is relatively short such that it does affect the pressure transients due to the subsequent buildup, drawdown type curves should not be used. In this case, pressure buildup type curves need to be generated to include the effect of producing time. This aspect of producing time and its effect on type curve analysis has been discussed recently by Raghavan.<sup>7</sup> Fig. 3, taken from his paper, presents buildup type curves for a vertically fractured well with infinite flow capacity fracture (for  $\kappa/\kappa_f = \infty$ ). Dimensionless pressure rise  $\bar{p}_{Df}$  has been plotted as a function of dimensionless shut-in time,  $\Delta t_{Df}$ . A family of type curves is shown with dimensionless producing time,  $Dx_f$  as a parameter. This figure clearly shows the limitations of drawdown type curves for analyzing pressure buildup data collected after small producing times. The effect of small producing time will not be considered in the subject study. However, a future paper is planned to cover this aspect.

#### b) Long producing time

If the producing time prior to shut-in is significantly long (that is  $(t_p + \Delta t)/\Delta t \approx 1$ ) so that it does not affect the pressure transients due to pressure buildup, drawdown type curves may be used to analyze pressure buildup data. This should be obvious from Fig. 3. The basis for this is depicted schematically in Fig. 4 in which the pressure behavior is shown during both constant rate drawdown and pressure buildup periods. According to the pressure transient theory  $\Delta p$  during pressure drawdown should be equal to that during the pressure buildup (for  $t = \Delta t$ ) provided they are defined as follows:

$$(\Delta p)_{\text{drawdown}} = p_i - p_{wf} \quad (6a)$$

$$= (\text{initial reservoir pressure}) \\ - (\text{wellbore flowing pressure})$$

$$(\Delta p)_{\text{buildup}} = p_{\Delta t} - p_{t_0} + \Delta t \quad (6b)$$

$$= (\text{shut-in pressure}) \\ - (\text{wellbore flowing pressure} \\ \text{in absence of shut-in})$$

However, since  $p_{t_0} + \Delta t$  is not readily available,  $(\Delta p)_{\text{buildup}}$  is normally defined as equal to

$$(p_{\Delta t} - p_{\Delta t=0})$$

Thus there is a difference between the  $(\Delta p)_{\text{drawdown}}$  and the way  $(\Delta p)_{\text{buildup}}$  are calculated. This difference is equal to  $(p_{\Delta t=0} - p_{t_0} + \Delta t)$  and is shown as the cross hatched area in Fig. 4.

To further investigate this difference, an MHF simulator<sup>2</sup> was used to simulate pressure buildup in an MHF gas well, using the liquid system analogy ( $\mu c_r = \text{constant}$ ). Reservoir and fracture data are shown in Table 1. The well was allowed to produce at a constant rate for 180 days followed by a pressure buildup test for 14 days. Pressure drawdown and buildup data expressed as  $\Delta[m(p)]/q$  as function of time ( $t$  or  $\Delta t$ ) in days are plotted on coordinate graph paper and are shown in Fig. 5.  $\Delta[m(p)]$  is defined as follows:

$$\Delta[m(p)]_{\text{drawdown}} = m(p_i) - m(p_{wf}) \quad (7a)$$

and

$$\Delta[m(p)]_{\text{buildup}} = m(p_{\Delta t}) - m(p_{\Delta t=0}) \quad (7b)$$

Note that there is virtually no difference between the drawdown and buildup data at early times. However, the difference gets bigger as time increases. This difference is due to the way  $\Delta[m(p)]_{\text{buildup}}$  is calculated. Also shown on Fig. 5 as the cross

hatched area is  $[m(p_{\Delta t=0}) - m(p_{t_0} + \Delta t)]$ , which is

equal to the above difference. Thus there is a basic difference between the drawdown and buildup type curves. However, in many cases this difference is not significant. This fact should also be apparent from Fig. 3 where the difference between the drawdown and buildup curve for long producing times is shown to be small. This indicates that in liquid systems, for large producing times, pressure buildup data can be analyzed using drawdown type curves to obtain reasonable answers.

## 2. Use of Liquid System Type Curves for Gas Wells

Next, we will examine the applicability of liquid system type curves for analyzing pressure drawdown and pressure buildup data obtained from real gas wells.

### a) Gas well drawdown data

To use the liquid system type curves for gas well drawdown data, it is recommended that real gas pseudo-pressure,  $m(p)$  is used in the dimensionless pressure ( $p_{wf}$ ) term and  $(\mu c_r)$  evaluated at the initial reservoir pressure is utilized in the dimensionless time ( $t_{D,r}$ ) term. Fig. 6 shows the comparison between the drawdown type curve for liquid and real gas systems. Drawdown data were generated using the MHF simulator and reservoir data shown in Table 1 and gas properties data shown in Table 2. Results indicate that the use of a liquid system type curve for gas well drawdown data is reasonable provided that the above mentioned conditions are met.

If one questions the applicability of these type curves for a particular gas reservoir because of unusual gas properties and/or reservoir pressure, as suggested in a recent paper<sup>3</sup>, type curves could be generated using an appropriate  $(\mu c_r)$  function, temperature, and pressure ranges specific to the reservoir under study. These type curves should then be used for pressure transient analysis of data from that reservoir.

### b) Gas well buildup data

To use the drawdown type curves for gas well buildup data, considerations regarding the duration of producing time, as discussed earlier, should also apply. Consequently, in this study it will be assumed that the effect of producing time on pressure buildup data is insignificant. The effect of the  $(\mu c_r)$  product on pressure buildup data will be mainly considered. As mentioned earlier, for pressure buildup analysis it is not clear as to the pressure level at which the  $(\mu c_r)$  product in the dimensionless time term should be evaluated.

To study this problem, the MHF simulator was utilized to generate pressure buildup data on an MHF gas well using real gas properties. Reservoir data and gas properties used are shown in Tables 1 and 2. As was done for the liquid case, the well was produced at a constant rate for 180 days followed by a pressure buildup for about 14 days. Pressure drawdown and buildup data expressed as  $\Delta[m(p)]/q$  as function of time in days are plotted and shown on Fig. 7. Note that this figure is similar to Fig. 5 presented earlier for the liquid case.  $\Delta[m(p)]$  has been appropriately defined. Also shown on Fig. 7,

as the cross hatched area, is  $[m(p_{\Delta t=0}) - m(p_{t_0} + \Delta t)]$ .

Notice that there is a marked difference between the drawdown and buildup type curve. This difference is much greater than that shown by the cross hatched area, mentioned above and discussed earlier.

The big difference in the drawdown and buildup curves for gas wells is due to large variations of  $(\mu c_r)$  or  $(\mu c_r)$  product as a function of pressure. For gas wells,  $(\mu c_r)$  is approximately equal to  $S \cdot (\mu c_r)$ . Fig. 8 shows the graph of  $(\mu c_r)$  vs pressure for the simulated gas well buildup case. Note that the variations in  $(\mu c_r)$  are much larger in the low pressure range (say below 2000 psi) than those in the high pressure range (say above 3000 psi). This indicates that during the pressure buildup, changes in the value of the  $(\mu c_r)$  product

will be more severe at a lower pressure than at a higher pressure. In the absence of the effect of producing time, this should explain the large difference between the drawdown and buildup curves.

The effects of variations of  $(\mu c_r)$  product as a function of pressure on drawdown data are well known in the petroleum industry. As early as 1962, Carter<sup>3</sup> proposed a method to find formation flow capacity based on dimensionless time correlation wherein viscosity and compressibility were point time functions. Al-Hussainy *et al.*<sup>4</sup> established that solutions for the flow of real gases should correlate as functions of dimensionless time based on initial values of viscosity and compressibility. Unfortunately, there is only limited work done to investigate the effect of  $(\mu c_r)$  variations on pressure buildup data in gas wells. Recently, Scott<sup>5</sup> suggested consideration of the variations of  $(\mu c_r)$  as point time functions in pressure buildup analysis of MHF gas wells.

During the course of this study, a new time function has been developed which takes into account the variations of  $(\mu c_r)$  product as a function of time and pressure. This function appears to provide excellent engineering answers when applied to gas well buildup data. This function will be discussed next.

REAL GAS PSEUDO-TIME,  $t_a(p)$

Al-Hussainy *et al.*<sup>4</sup> defined real gas pseudo-pressure,

$$m(p) = 2 \int_{p_0}^p \frac{p}{\mu(p)z(p)} dp \quad (8)$$

which takes into account the variations of gas viscosity and z-factor as a function of pressure with  $p_0$  as a low base pressure.

In this paper an analogous function is defined as follows:

$$E_a(t) = \int_{t_0}^t \frac{dt}{\bar{\mu}(t)\bar{z}_c(t)} \quad (9)$$

where  $\bar{\mu}$  and  $\bar{z}_c$  are used to denote viscosity and system compressibility as a function of time rather than  $\mu$  and  $c_r$  which are usually expressed as functions of pressure. If  $E_a(t)$  is redefined as a function of pressure, a new function is obtained as

$$t_a(p) = \int_{p_0}^p \frac{\left[ \frac{dt}{dp} \right]}{\mu(p)c_c(p)} dp \quad (10)$$

where  $\mu$  and  $c_r$  are functions of pressure. This function is referred to as real gas pseudo-time,  $t_a(p)$ , in this paper.

If time and pressure are assumed to vary linearly with each other, over small time increments, Eq. 10 can be approximated as

$$t_a(p) \approx \sum_{j=1}^n \frac{(t_j - t_{j-1})}{(p_j - p_{j-1})} \int_{p_{j-1}}^{p_j} \frac{dp}{\mu(p)c_c(p)} \quad (11)$$

Note that in Eq. 11,  $t_j$  represents flowing time for a drawdown test and shut-in time for a buildup test. Eq. 11 may be rewritten as

$$t_a(p) \approx \sum_{j=1}^n \frac{(t_j - t_{j-1})}{(p_j - p_{j-1})} [I(p_j) - I(p_{j-1})] \quad (12)$$

where an integral

$$I(p) = \int_{p_0}^p \frac{dp}{\mu(p)c_c(p)} \quad (13)$$

can be evaluated beforehand using  $\mu$  and  $c_r$  as functions of pressure. In Eq. (13),  $p_0$  is a low base pressure and  $p$  is the maximum pressure of interest. The above integral, expressed in graphical or tabular form, can be used in conjunction with Eq. 12 to compute real gas pseudo time,  $t_a(p)$ . Since  $c_r$  rather than  $c_c$  is normally available as a function of pressure, the following relationships may be utilized.

$$c_c = S_g c_g + S_o c_o + S_w c_w + c_f \quad (14)$$

For a gas well, Eq. 14 is usually approximated as

$$c_c \approx S_g c_g \quad (15)$$

Going back to Eq. 11, it should be noted that during the time interval,  $\Delta t_j = t_j - t_{j-1}$  and the pressure change,  $\Delta p_j = p_j - p_{j-1}$ , the viscosity-compressibility product  $(\mu c_c)_j$  is defined by

$$\frac{1}{(\mu c_c)_j} = \frac{1}{\Delta p_j} \int_{p_{j-1}}^{p_j} \frac{dp}{\mu(p)c_c(p)} \quad (16)$$

where,  $j = 1, 2, \dots, n$

This definition in Eq. 11 gives

$$t_a(p) \approx \sum_{j=1}^n \frac{\Delta t_j}{(\mu c_t)_j} \quad (17)$$

Eq. 17 clearly indicates that the units in  $t_a(p)$  consist not only of time but a combination of time, viscosity, and compressibility.

#### COMPUTATION OF REAL GAS PSEUDO-TIME, $t_a(p)$

Since Eq. 12 for  $t_a(p)$  contains an integral,  $I(p)$ , given by Eq. 13, computation can be performed using either graphical or tabular data. Simply, it can be accomplished by means of a computer or a desk calculator. Trapezoidal or Simpson's rule can be used. Integration can be performed by reading mid-point values of  $(1/\mu c_t)$  from the table or graph and multiplying by  $\Delta p$ . Computations of  $I(p)$  utilizing gas properties in Table 2 are outlined in Table 3. Fig. 9 shows a graph of  $(1/\mu c_t)$  and  $I(p)$  as a function of pressure. Although not shown, it is also useful to prepare a similar graph for real gas pseudo-pressure,  $m(p)$ . Thus  $I(p)$  and  $m(p)$  curves prepared for the gas in a specific reservoir can be used as master graphs for future wells in that reservoir. The  $I(p)$  curve is used in conjunction with Eq. 12 to convert real times to corresponding pseudo-times for the specific application.

#### CERTAIN USEFUL ASPECTS OF $t_a(p)$

Before discussing the application, let us consider certain aspects of real gas pseudo-time,  $t_a(p)$ :

##### Definition of dimensionless time

If  $t_a(p)$  is used to express the dimensionless time term,  $t_{Dax_f}$ , then

$$t_{Dax_f} = \frac{2.634 \times 10^{-4} k}{\phi x_f^2} t_a(p) \quad (18)$$

Since the viscosity-compressibility product is already included in  $t_a(p)$ , it does not appear in Eq. (18). To express an analogy between Eq. 18 and Eq. 2, the above equation can be multiplied and divided by  $(\mu c_t)_i$ , evaluated at the initial reservoir pressure. This provides

$$t_{Dax_f} = \frac{2.634 \times 10^{-4} k}{\phi (\mu c_t)_i x_f^2} [(\mu c_t)_i \cdot t_a(p)] \quad (19)$$

It should be noted that in Eqs. 18 and 19, a general definition of dimensionless time,  $t_{Dax_f}$  has been used. Accordingly, it may represent dimensionless drawdown time or dimensionless buildup time depending on whether  $t_a(p)$  in Eq. 12 has been calculated using the flowing time,  $t$ , or shut-in time,  $\Delta t$ .

Eq. 19 appears very similar to Eq. 2 where time ( $t$ ) has been replaced by  $[(\mu c_t)_i \cdot t_a(p)]$ . This suggests a correspondence between the real time and the pseudo-time. This also implies some correspondence between the flowing time for a drawdown test and the shut-in time for a buildup test as well be shown next.

#### Correspondence between flowing and shut-in times

The subject correspondence is being established based on certain observations rather than rigorous mathematical solutions.

Although the use of the real gas pseudo-time,  $t_a(p)$  is not meant to be restricted, this study points out that the dimensionless time (see Eq. 18 or 19) for gas well buildup data correlates much better as a function of  $t_a(p)$ .

Based on the earlier work of Al-Hussainy et al.<sup>6</sup>, it appears reasonable to assume that the dimensionless time for pressure drawdown data should correlate as a function of the  $(\mu c_t)_i$  product evaluated at the initial reservoir pressure as shown in Eq. 2.

A comparison between Eq. 2 and Eq. 18 or 19 imply the following correspondence between the flowing time,  $t$ , and the shut-in time,  $\Delta t$ :

$$\frac{t}{(\mu c_t)_i} = t_a(p) \quad (20)$$

or,

$$t = [(\mu c_t)_i \cdot t_a(p)] \quad (21)$$

It should be noted that the shut-in time,  $\Delta t$ , is already included in  $t_a(p)$ . The use of the above concept appears to provide a number of practical benefits.

1. This allows us to use the same definition of the dimensionless time (see Eqs. 2 and 19) in type curve analysis for both pressure drawdown and buildup data.
2. In performing type curve analysis of the combined pressure drawdown and buildup data from the same well, it is possible to plot drawdown data as a function of time ( $t$ ) and buildup data as a function of  $[(\mu c_t)_i \cdot t_a(p)]$  using the same graph or tracing paper. This concept, along with the superposition principle, was utilized in a companion paper by Bostic et al.<sup>10</sup>
3. This also permits us to compare drawdown and buildup data from the same gas well, as shown in Fig. 10. This will be discussed next showing the application of  $t_a(p)$ .

#### APPLICATION OF REAL GAS PSEUDO-TIME, $t_a(p)$

To illustrate the application of real gas pseudo-time, let us consider the pressure drawdown and buildup data, shown in Fig. 7, for the gas well

case. These data have been replotted in Fig. 10 and are shown as  $\Delta[m(p)]/q$  as a function of time ( $t$  or  $\Delta t$ ) in days. In this figure, solid line with circles represent the drawdown data whereas the solid line with triangles is for the buildup data. As mentioned earlier, there is a considerable difference between the two curves. These buildup data, being so much on the right side of the drawdown curve, imply that the use of  $(\mu_c)$  at the initial reservoir pressure will result in computed fracture length which is much greater than the actual. This aspect will be investigated later by means of type curve analysis.

To use the concept of real gas pseudo-time, Eq. 12 was used in conjunction with Fig. 9 to convert shut-in time,  $\Delta t$ , to  $t_a(p)$ . Eq. 21 was utilized to express these data in terms of equivalent flowing time,  $t$  or  $(\mu_c) \cdot t_a(p)$ . It enabled us to compare drawdown and buildup data on an equivalent time basis. Pressure buildup data plotted as a function of  $(\mu_c) \cdot t_a(p)$  are shown as the dotted line with triangles. Note that the result was to move the buildup data (shown as triangles) horizontally from the solid line on the right to the dotted line on the left. Also the modified buildup curve came very close to the drawdown curve. This figure also indicates that real shut-in times,  $\Delta t$ , are equivalent to only about 60% of the equivalent flowing times,  $t$ . For example, the real shut-in time of 6 days is equal to only about 3.75 days of the equivalent flowing time. It is possible to plot shut-in time,  $\Delta t$  as a function of equivalent flowing time,  $(\mu_c) \cdot t_a(p)$ . This is shown in Fig. 11. The solid line represents the gas case and the dotted line is for liquid case. This figure clearly shows that shut-in times for liquid case are equal to the equivalent flowing times, whereas they are much less for the gas case. This indicates that a graph similar to Fig. 11 should also prove useful in the design of a pressure buildup test on an MHF gas well. For example, if a pressure buildup test is required to be run for an equivalent flowing time of 6 days to obtain the desired information, it may be necessary to run the test for about 10 days, which is almost twice as long.

Let us next consider the effect of  $(\mu_c)$  product evaluated at different pressure levels on the type curve analysis of gas well buildup data. The values of computed fracture lengths will be compared against the actual total fracture length of 1000 feet used in the simulator. Pressure drawdown and buildup data presented in the preceding example will be utilized for this purpose. Fig. 12 shows a semi-log graph of pressure buildup and drawdown data expressed in dimensionless quantities. Dimensionless pressure,  $p_{wD}$ , has been plotted as a function of dimensionless time,  $Dx_D$ . For drawdown data,  $(\mu_c)$  product in the dimensionless time was evaluated at the initial reservoir pressure. This curve will be considered as the reference type curve.

Data curves for buildup data have been plotted using the  $(\mu_c)$  product at the initial reservoir pressure,  $p_i$ , and the final wellbore flowing pressure prior to shut-in,  $p_{\Delta t=0}$ . Since the data curve using  $(\mu_c)$  is on the right-hand side of the drawdown type curve, matching will provide computed fracture length which is greater than the actual. On the other hand, the data curve using  $\mu_c$  at  $p_{\Delta t=0}$  being on the left-hand side of the reference

type curve, provided a computed fracture length which is smaller than the actual. A third data curve is also shown which utilized Eq. 18 to incorporate the concept of real gas pseudo-time function. Results of curve matching, using the new time function, gave results which are close to the actual fracture length.

Table 4 provides a comparison of fracture lengths, computed by type curve analysis, using the  $(\mu_c)$  product in the dimensionless time term at various pressure levels. Results of four sets of simulated gas well buildup data are shown, where both the value of fracture length and the level of final flowing pressure  $p_{\Delta t=0}$  were varied. Inspection of Table 4 reveals that results are affected by the  $(\mu_c)$  product used and the level of the final flowing pressure at the instant of shut-in. The use of  $(\mu_c)$ , provided values of computed fracture length which are too optimistic. The effect is further exaggerated at a lower value of the flowing pressure. The use of the  $(\mu_c)$  product at  $p_{\Delta t=0}$  provides a low but reasonable value if  $p_{\Delta t=0}$  is relatively high, otherwise it provides pessimistic values of fracture length. The use of real gas pseudo-time provided computed fracture length values similar to those entered in the simulator. Based on a number of computer runs, it appears that the concept of real gas pseudo-time function is useful in analyzing post-treatment buildup data from fractured (including MHF) gas wells.

#### Steps Used in Applying Real Gas Pseudo-Time Function for Type Curve Matching

The following step-by-step procedure should be useful in applying the concept of real gas pseudo-time to gas well buildup data for type curve matching purposes.

##### Step 1

Prepare a table of gas properties as shown in Table 2. Compute real gas pseudo-pressure,  $m(p)$  and integral,  $I(p)$  as a function of pressure and plot them on coordinate graph paper.

##### Step 2

Tabulate pressure buildup data,  $p_{\Delta t}$  vs  $\Delta t$ .

Using the above figure, convert  $p_{\Delta t}$  to  $m(p_{\Delta t})$  and compute  $\Delta[m(p)] = m(p_{\Delta t}) - m(p_{\Delta t=0})$ .

##### Step 3

Using the figure for  $I(p)$  and Eq. 12 convert  $\Delta t$  to  $t_a(p)$ . It should be noted that  $t_a(p)$  already contains the  $(\mu_c)$  product.

##### Step 4

Plot  $\Delta[m(p)]$  vs  $t_a(p)$  on a tracing paper utilizing the appropriate type curve. Type curve matching should be done in the usual manner. For an MHF well, if formation flow capacity is known a priori, the vertical position of the data plot may be fixed on the y-axis of the type curve. Otherwise the matching should be done by sliding the tracing paper parallel to both x and y axes.

**Step 5**

Once a match is obtained and a match point is selected, the fracture length is calculated as

$$x_f = \sqrt{\frac{2.634 \times 10^{-4} k}{\phi} \frac{[c_a(p)]_M}{[c_{Dax_f}]_M}} \quad (22)$$

In regard to the  $\phi$  term in the above equation, the following should be pointed out:

If the  $(\mu c_r)$  product in the real gas pseudo-time,  $t_a(p)$ , is based on the system compressibility,  $c_s = g_a c_g + S_c + S_v c_v + c_r$ , then  $\phi$  should be the total porosity in the system.

If gas compressibility,  $c_g$ , has been used instead of  $c_r$ , then  $\phi$  should be replaced by hydrocarbon porosity,  $\phi_g$ .

Once the value of  $x_f$  is determined, the fracture flow capacity can be determined by Eq. 3 as

$$(k_f v) = (F_{CD})(k x_f) \text{ md-ft} \quad (23)$$

**CONCLUDING REMARKS**

As a result of this study, the following remarks appear warranted:

1. A new time function [real gas pseudo-time,  $t_a(p)$ ] has been developed which has aided in post-treatment pressure buildup analysis of fractured (including MHF) gas wells.
2. This function is analogous to the real gas pseudo-pressure,  $m(p)$  of Al-Hussainy *et al.*<sup>4</sup> Although it is not a rigorous function, it provides excellent engineering answers for vertically fractured gas well buildup analysis.
3. There is a basic difference between the drawdown type curve and the buildup type curve because of the different ways  $\Delta[m(p)]$  or  $\Delta p$  are calculated for pressure drawdown and buildup. However, drawdown type curves may be used for buildup data provided the producing time prior to shut-in is long (that is  $(t_p + \Delta t)/\Delta t \approx 1$ ).
4. For small producing time prior to shut-in, buildup data should not be analyzed by drawdown type curves.
5. To use liquid system type curves for gas wells, the following points should be noted:
  - a) For analyzing gas well drawdown data, the use of liquid system type curves appears reasonable provided that the real gas pseudo-pressure is used in the dimensionless pressure term and the  $(\mu c_r)$  product in the dimensionless time is evaluated at the initial reservoir pressure. However in certain cases, because of unusual gas properties or reservoir pressure, type curves should be generated using the appropriate  $(\mu c_r)$  function, temperature, and

pressure ranges and then used for the specific application.

- b) For gas well buildup data, the use of  $(\mu c_r)$  product at the initial reservoir pressure provides optimistic values for fracture lengths whereas the  $(\mu c_r)$  at the final flowing pressure provides pessimistic values for fracture length. The use of the real gas pseudo-time provides satisfactory values of fracture length.
6. Due to the effect of variations of  $(\mu c_r)$  on gas well buildup data, it may be necessary to run a buildup test twice as long as it is normally run. This aspect should be considered in the design of pressure buildup tests on MHF gas wells.
  7. Although the discussion in this paper is limited to pressure buildup analysis of vertically fractured gas wells, the utility of the real gas pseudo-time is not meant to be restricted to such wells only. For example, this function was also found very useful for gas wells in analyzing wellbore storage data, linear flow data, etc., to name a few.

**NOMENCLATURE**

$c_f$	= formation compressibility, $\text{psi}^{-1}$ ( $\text{Pa}^{-1}$ )
$c_g$	= gas compressibility, $\text{psi}^{-1}$ ( $\text{Pa}^{-1}$ )
$c_o$	= oil compressibility, $\text{psi}^{-1}$ ( $\text{Pa}^{-1}$ )
$c_s$	= system compressibility, $\text{psi}^{-1}$ ( $\text{Pa}^{-1}$ )
$\bar{c}_t$	= system compressibility as a function of time, $\text{psi}^{-1}$ ( $\text{Pa}^{-1}$ )
$c_v$	= water compressibility, $\text{psi}^{-1}$ ( $\text{Pa}^{-1}$ )
$F_{CD}$	= dimensionless fracture flow capacity (see Eq. 3)
$h$	= formation thickness, ft (m)
$I(p)$	= integral in Eq. 13, $\text{psi}^2/\text{cp}$ ( $\text{Pa}^2/\text{s}$ )
$k$	= formation permeability, md ( $10^{-3} \mu\text{m}^2$ )
$k_f$	= fracture permeability, md ( $10^{-3} \mu\text{m}^2$ )
$m(p)$	= real gas pseudo-pressure, $\text{psi}^2/\text{cp}$ ( $\text{MPa}^2/\text{pa}\cdot\text{s}$ ) (see Eq. 8)
$\Delta[m(p)]$	= difference in real gas pseudo-pressures $\text{psi}^2/\text{cp}$ ( $\text{MPa}^2/\text{Pa}\cdot\text{s}$ )
$p$	= pressure, psi (MPa)
$p_i$	= initial pressure, psi (MPa)
$p_{\Delta t}$	= shut-in pressure, psi (MPa)

$P_{\Delta t=0}$	= shut-in pressure at the instant of shut-in, psi (MPa)
$\bar{P}_{Da}$	= dimensionless shut-in pressure rise (see Ref. 7)
$P_{wD}$	= dimensionless pressure or pressure drop (see Eq. 1)
$P_{wf}$	= wellbore flowing pressure, psi (MPa)
$\Delta p$	= pressure change, psi (MPa)
$\Delta p_j$	= pressure change, $p_j - p_{j-1}$ , psi (MPa) (see Eq. 11)
$\Delta(p^2)$	= difference in squares of pressures, $\text{psi}^2$ (MPa <sup>2</sup> )
$q$	= flow rate, MCF/D ("standard" $\text{m}^3/\text{d}$ )
$S$	= saturation, fraction
$S_g$	= gas saturation, fraction
$S_o$	= oil saturation, fraction
$S_w$	= water saturation, fraction
$t$	= flowing time, hours
$t_a(p)$	= real gas pseudo-time, hours-psi/cp (hours-Pa/Pa·s) (see Eq. 11)
$[t_a(p)]_M$	= real gas pseudo-time for match point, hours-psi/cp (hours-Pa/Pa·s)
$f_a(t)$	= a function defined by Eq. 9
$t_{Dx_f}$	= dimensionless time based on $x_f$ (see Eq. 2)
$\Delta t_{dx_f}$	= dimensionless shut-in time (see Ref. 7)
$t_{Dax_f}$	= dimensionless time based on $t_a(p)$ (see Eqs. 18 and 19)
$[t_{Dax_f}]_M$	= dimensionless time based on $t_a(p)$ for match point (see Eq. 22)
$t_p$	= producing time prior to buildup, hours
$\Delta t$	= shut-in time, hours
$\Delta t_j$	= time interval, $t_j - t_{j-1}$ , hours
$T$	= reservoir temperature, °R (K)
$x_e$	= distance from well to the reservoir boundary, ft (m)
$x_f$	= fracture half length, ft (m)
$z$	= real gas deviation factor
$\mu$	= viscosity, cp (Pa·s)
$\bar{\mu}$	= viscosity as a function of time, cp (Pa·s)

$(\mu c_e)$  = viscosity-compressibility product, cp/psi(Pa·s/Pa)

$(\mu c_e)_i$  = viscosity-compressibility product at initial reservoir pressure, cp/psi(Pa·s/Pa)

$(\mu c_e)_j$  = viscosity-compressibility product in a given interval, cp/psi(Pa·s/Pa) (see Eq. 16)

$\Delta$  = delta or difference

$\phi$  = formation porosity, fraction

$\Sigma$  = sigma or summation

#### Subscripts

$cD$  = dimensionless flow capacity

$D$  = dimensionless

$Dx_f$  = dimensionless based on  $x_f$  and time

$Dax_f$  = dimensionless based on  $x_f$  and pseudo-time

$a$  = apparent or pseudo

$e$  = external boundary

$f$  = fracture or formation

$g$  = gas

$i$  = initial

$j$  = index for summation

$M$  = match point values

$n$  = index for summation

$o$  = oil

$p$  = producing

$t$  = total

$w$  = water

$wf$  = wellbore flowing

#### REFERENCES

1. Earlougher, R. C., Jr.: Advances in Well Test Analysis, Monograph Series, Society of Petroleum Engineers of AIME, Dallas (1977) 2, 264.
2. Agarwal, R. G., Carter, R. D., and Pollock C. B.: "Evaluation and Performance Prediction of Low-Permeability Gas Wells Stimulated by Massive Hydraulic Fracturing," J. Pet. Tech. (March, 1979) 362-372.
3. Cinco-L., H., Samaniego-V., F., and Dominguez-A., N.: "Transient Pressure Behavior for a Well With a Finite Conductivity Vertical Fracture," Soc. Pet. Eng. J. (August, 1978) 253-264.

<p>4. Al-Hussainy, R., Ramey, H. J. Jr., and Crawford, P. B.: "The Flow of Real Gases Through Porous Media," <u>J. Pet. Tech.</u> (May, 1966) 624-636; <u>Trans., AIME</u>, 237.</p> <p>5. Al-Hussainy, R. and Ramey, H. J. Jr.: "Application of Real Gas Flow Theory to Well Testing and Deliverability Forecasting," <u>J. Pet. Tech.</u> (May, 1966) 637-642; <u>Trans., AIME</u>, 237.</p> <p>6. Gringarten, A. C., Ramey, H. J. Jr., and Raghavan, R.: "Unsteady-State Pressure Distribution Created by a Well With a Single Infinite-Conductivity Vertical Fracture," <u>Soc. Pet. Eng. J.</u> (August 1974) 347-360; <u>Trans., AIME</u>, 257.</p> <p>7. Raghavan, R.: "The Effect of Producing Time on Type Curve Analysis," submitted to SPE of AIME.</p>	<p>8. Carter, R. D.: "Solutions of Unsteady-State Radial Gas Flow," <u>J. Pet. Tech.</u> (May, 1962) 559-554; <u>Trans., AIME</u>, 225.</p> <p>9. Scott, J. O.: "Application of a New Method for Determining Flow Characteristics of Fractured Gas Wells in Tight Sands," paper presented at 1979 SPE Symposium on Low Permeability Gas Reservoirs, Denver, Colo., May 20-22, 1979.</p> <p>10. Bostic, J. N., Agarwal, R. G., and Carter, R. D.: "Combined Analysis of Post-Fracturing Performance and Pressure Buildup Data for Evaluating an MHF Gas Well," paper SPE 8280 presented at SPE 54th Annual Fall Meeting, Las Vegas, Nev., Sept. 23-26, 1979.</p>
--	---

TABLE 1Reservoir and Fracture Data for Simulated MHF WellReservoir Data

Reservoir pressure, $p_i$	5000 psi (34.5 MPa)
Reservoir temperature, $T$	720 °R (400°K)
Formation thickness, $h$	50 ft (15.2m)
Formation permeability, $k$	.01 md ( $9.9 \times 10^{-6} \mu\text{m}^2$ )
Formation porosity, $\phi$	.07 fraction
Initial gas saturation, $S_g$	.50 fraction
Production Rate, $q$	500 Mcf/D ( $14,158\text{m}^3 / \text{D}$ )

Fracture Data

Total fracture length, $2x_f$	1000 ft (305m)
Fracture flow capacity, $k_{fw}$	50 md-ft ( $15 \times 10^3 \mu\text{m}^2\text{m}$ )
Dimensionless fracture capacity, $F_{CD}$	10

**TABLE 2**

**Gas Properties for Simulated MHF Gas Well**

Pressure (psi)	Viscosity (cp)	z-factor (fraction)	$c_g$ ( $\text{psi}^{-1}$ )	$m(p)$ ( $\text{psi}^2/\text{cp}$ )
0	--	1.000	--	--
600	.0147	.971	$170.6 \times 10^{-5}$	$2.5 \times 10^7$
1200	.0155	.951	$86.0 \times 10^{-5}$	$10.0 \times 10^7$
1800	.0166	.940	$56.0 \times 10^{-5}$	$21.8 \times 10^7$
2400	.0180	.939	$40.9 \times 10^{-5}$	$37.3 \times 10^7$
3000	.0197	.947	$31.1 \times 10^{-5}$	$55.6 \times 10^7$
3600	.0216	.964	$24.3 \times 10^{-5}$	$75.6 \times 10^7$
4200	.0236	.986	$19.5 \times 10^{-5}$	$96.9 \times 10^7$
4800	.0255	1.014	$16.0 \times 10^{-5}$	$118.9 \times 10^7$
5400	.0275	1.045	$13.3 \times 10^{-5}$	$141.3 \times 10^7$

**TABLE 3**

Computation of  $\frac{1}{\mu c_p}$  and  $1/\mu_p = \int_0^{5400} \frac{dp}{\mu(p) c_p(p)}$  Using Gas Properties

Pressure (psi)	$\mu c_p^*$ (cp/psi)	$(1/\mu c_p)$ (psi/cp)	Mean ( $1/\mu c_p$ ) (psi/cp)	$\Delta p$ (psi)	Mean ( $1/\mu c_p$ ) X $\Delta p$ (psi <sup>2</sup> /cp)	$1/\mu_p^{**}$ (psi <sup>2</sup> /cp)
0	-	-	-	-	-	0.00
600	$12.54 \times 10^{-6}$	$7.98 \times 10^4$	$3.99 \times 10^4$	600	$2.39 \times 10^7$	$2.39 \times 10^7$
1200	$6.67 \times 10^{-6}$	$15.00 \times 10^4$	$11.49 \times 10^4$	600	$6.89 \times 10^7$	$9.28 \times 10^7$
1800	$4.70 \times 10^{-6}$	$21.29 \times 10^4$	$18.15 \times 10^4$	600	$10.89 \times 10^7$	$20.17 \times 10^7$
2400	$3.68 \times 10^{-6}$	$27.17 \times 10^4$	$24.23 \times 10^4$	600	$14.54 \times 10^7$	$34.71 \times 10^7$
3000	$3.06 \times 10^{-6}$	$32.64 \times 10^4$	$29.91 \times 10^4$	600	$17.95 \times 10^7$	$52.66 \times 10^7$
3600	$2.62 \times 10^{-6}$	$38.14 \times 10^4$	$35.37 \times 10^4$	600	$21.22 \times 10^7$	$73.88 \times 10^7$
4200	$2.30 \times 10^{-6}$	$43.46 \times 10^4$	$40.78 \times 10^4$	600	$24.47 \times 10^7$	$98.35 \times 10^7$
4800	$2.04 \times 10^{-6}$	$49.02 \times 10^4$	$46.24 \times 10^4$	600	$27.74 \times 10^7$	$126.09 \times 10^7$
5400	$1.83 \times 10^{-6}$	$54.68 \times 10^4$	$51.85 \times 10^4$	600	$31.11 \times 10^7$	$157.20 \times 10^7$

\*  $\mu c_p^* = S_g \mu c_p$

\*\*  $1/\mu_p$  vs. pressure is shown in Fig. 9

Remarks: Real gas pseudo pressure,  $1/\mu_p$  can be computed using Eq. 12 and  $1/\mu_p$  in conjunction with the desired pressure vs. time data.

**TABLE 4**

Comparison of Computed Fracture Lengths from Type Curve Analysis of Gas Well Buildup Data Using  $\mu c_p^*$  Product at Various Pressure Levels

Run No.	Flow Rate (MCF/D)	Initial Pressure (psi)	Final Flowing Pressure (psi)	Total Fracture Length (ft)		
				Simulator	$\mu c_p^*$	$\mu c_p^*$ at $\beta = 1 = 0$
1A	500	5000	2374	1000	1370	1022
1B	650	5000	1332	1000	960	605
2A	500	5000	2245	1500	1430	1515
2B	650	5000	1163	1500	2866	1515

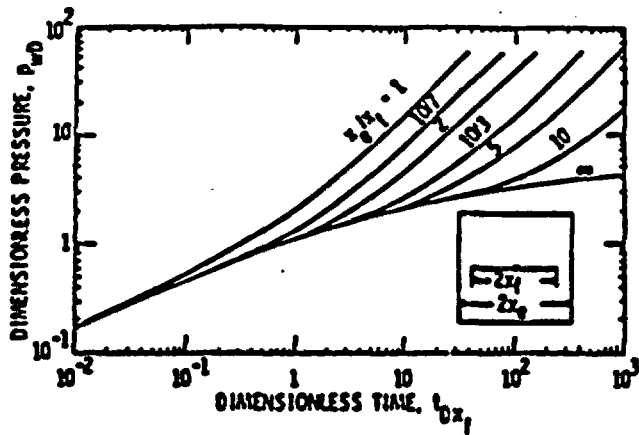


Fig. 1 - Constant rate drawdown type curves for infinite flow capacity vertical fracture - liquid system (after Gringarten & Li, 1967)

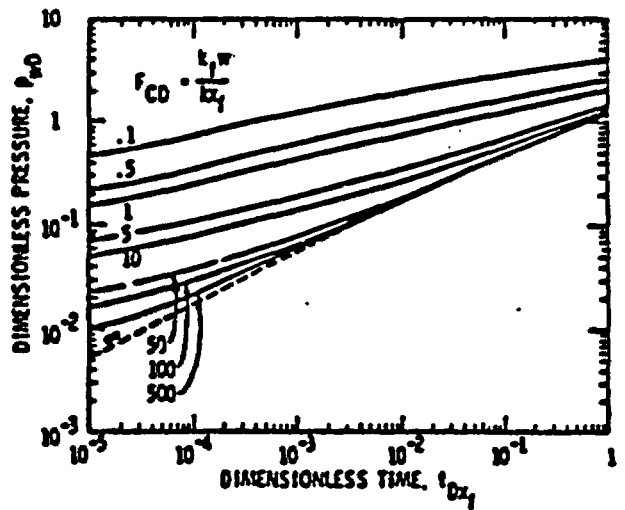


Fig. 2 - Constant rate drawdown type curves for finite flow capacity vertical fractures - liquid system (after Agarwal & Li, 1972)

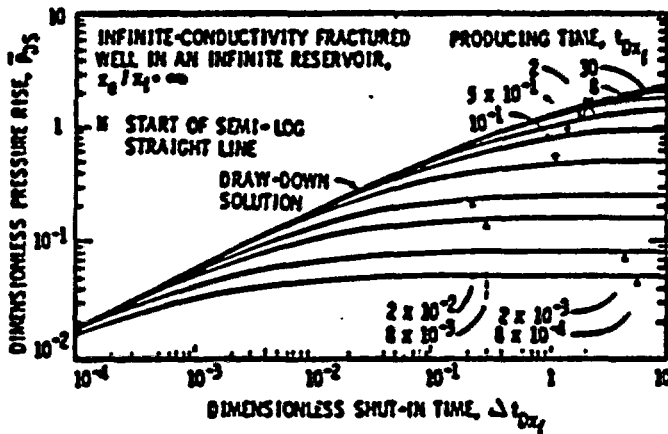


Fig. 3 - Effect of producing time on buildup data for infinite flow capacity vertical fracture - liquid system (after Raghavan, 1971)

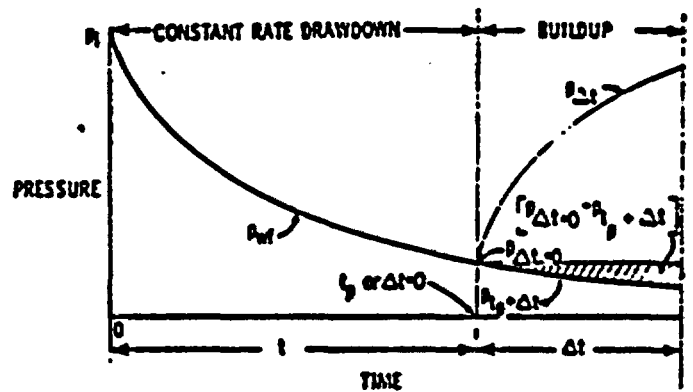


Fig. 4 - Schematic of pressure behavior during constant rate drawdown and buildup periods.

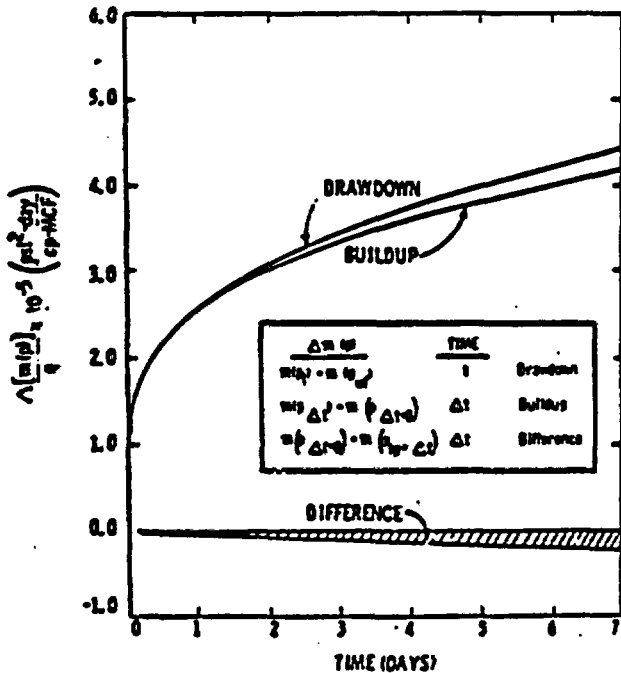


Fig. 5 - Pressure drawdown and buildup data vs time (liquid system -  $c_e$  is constant).

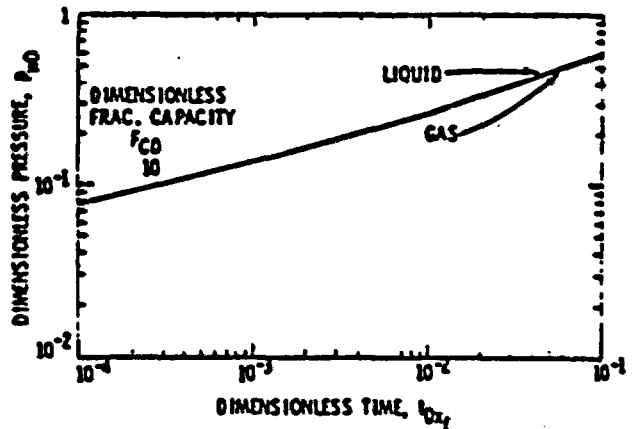


Fig. 6 - Comparison between drawdown type curves for liquid and gas systems (constant well rate).

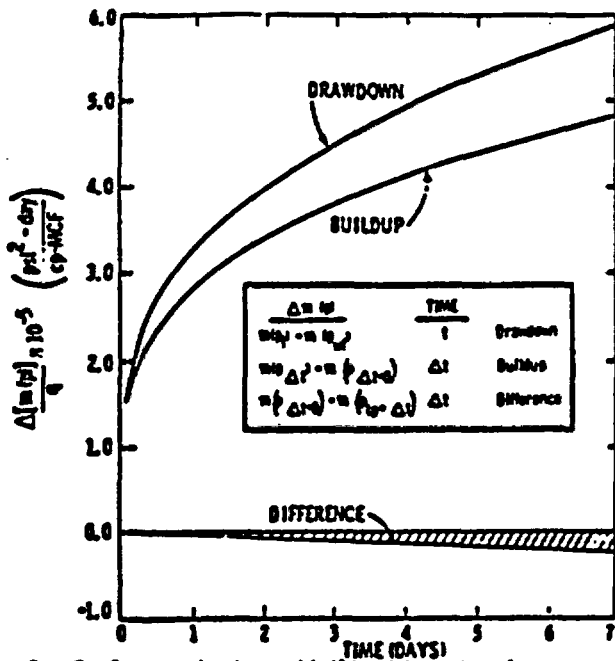


Fig. 7 - Pressure drawdown and buildup data vs time (gas system -  $c_e$  is function of pressure).

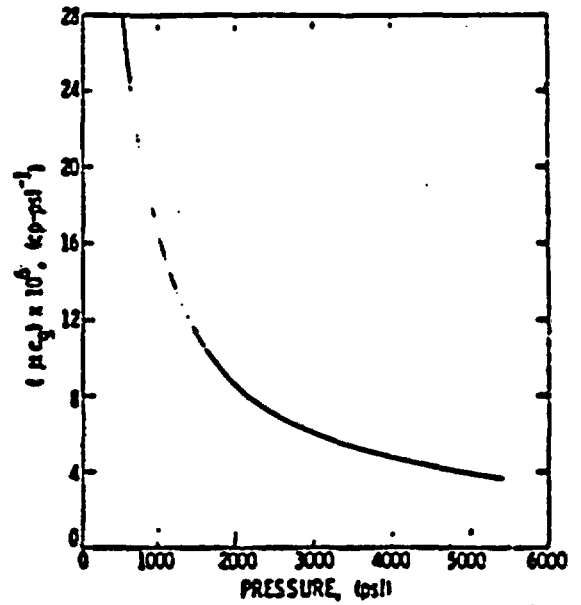


Fig. 8 - Variations of gas viscosity-compressibility ( $= c_e$ ) product as a function of pressure.

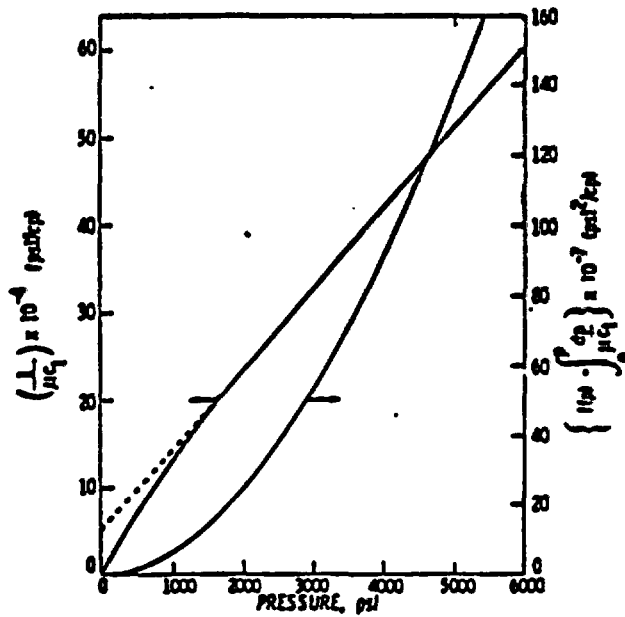


Fig. 9 -  $\frac{1}{c_e}$  and  $I(p) = \int_0^p \frac{dp}{\mu c_e}$  as a function of pressure.

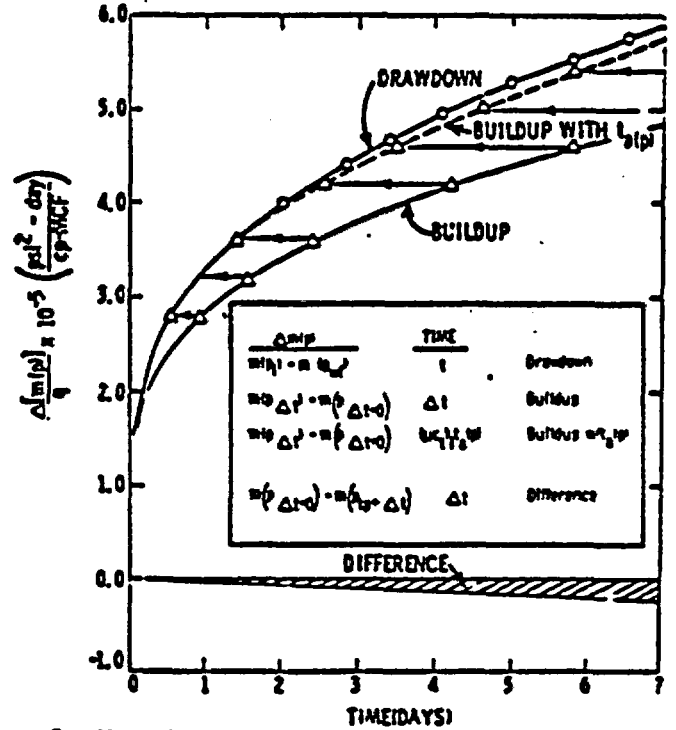


Fig. 10 - Application of real gas pseudo-time to gas well buildup data.

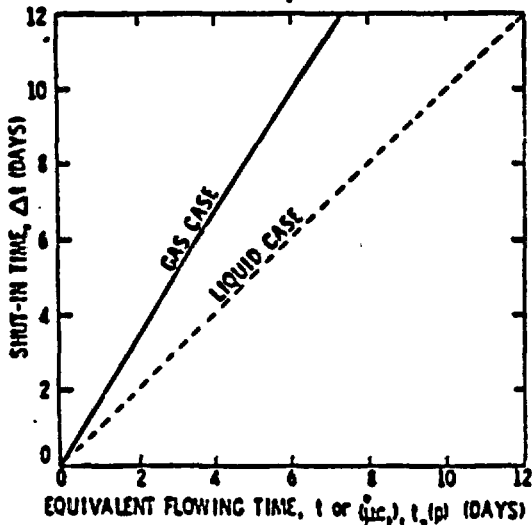


Fig. 11 - Shut-in time vs equivalent flowing time.

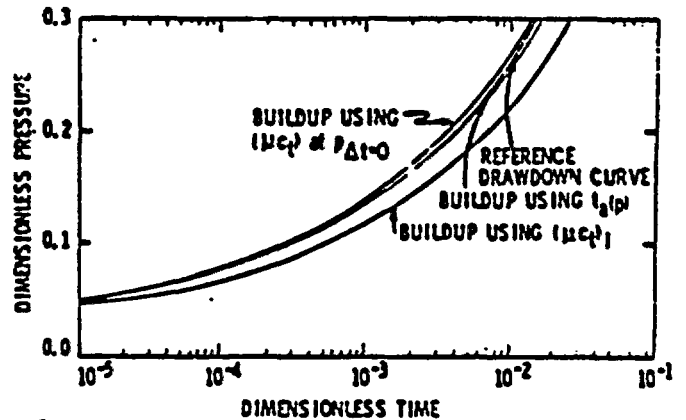


Fig. 12 - Drawdown and buildup data plotted using ( $= c_e$ ) at different pressure levels (gas case -  $c_e$  is a fn. of pressure).

20002

REV. 2

U.S. GEOLOGICAL SURVEY  
WATER RESOURCES DIVISION  
COLORADO WATER  
RESOURCES LIBRARY

NNWSI PROJECT

UNITED STATES GEOLOGICAL SURVEY

DENVER, COLORADO

DETAILED PROTOTYPE TEST PLAN

CROSS-HOLE PNEUMATIC AND HYDRAULIC TESTING  
IN SUPPORT OF EXPLORATORY SHAFT HYDROLOGIC TESTING

WBS 1.2.6.9.4.2.4

Principal Investigator - Robert C. Trautz

Co-Investigator - Robert W. Craig

<u>Principal Investigator</u>	<u>Date</u>	<u>Co-Investigator</u>	<u>Date</u>
Robert C. Trautz		Robert W. Craig	

<u>Technical Reviewer</u>	<u>Date</u>	<u>Chief, Branch of NNWSI</u>	<u>Date</u>
Sandi Doty		Larry R. Hayes	

8.3.1.2.2.3  
Encl. 2

**U.S. GEOLOGICAL SURVEY  
WATER RESOURCES DIVISION  
COLORADO WATER  
RESOURCES LIBRARY**

**TABLE OF CONTENTS**

	<b>PAGE</b>
<b>7.0 NONCONFORMANCE ACTIONS</b>	<b>2.4-75</b>
<b>8.0 DOCUMENTATION</b>	<b>2.4-75</b>
<b>9.0 SAFETY</b>	<b>2.4-75</b>
<b>10.0 REPORTS</b>	<b>2.4-76</b>
10.1 PRELIMINARY REPORTS	2.4-76
10.2 FINAL REPORT	2.4-77
<b>11.0 DEFINITIONS</b>	<b>2.4-78</b>
<b>12.0 REFERENCES</b>	<b>2.4-79</b>
12.1 PROGRAM REFERENCES	2.4-79
12.2 TECHNICAL REFERENCES	2.4-79
<b>13.0 APPENDIX A - CROSS-HOLE PNEUMATIC AND HYDRAULIC PROTOTYPE TEST SCHEDULES AND MILESTONES</b>	<b>2.4-82</b>
<b>14.0 APPENDIX B - APPLICABLE TECHNICAL PROCEDURES CURRENTLY AVAILABLE FOR USE</b>	<b>2.4-87</b>

LIST OF FIGURES (CONTINUED)

FIGURE		PAGE
2.4-14	VERTICAL CROSS-SECTION THROUGH AXIS OF FLOW DOMAIN SHOWING MESH SIZE OF LARGE AND SMALL GRIDS AND LOCATION OF LINE SEGMENT AB	2.4-63
2.4-15	NUMERICALLY DERIVED PRESSURE DISTRIBUTIONS ALONG LINE SEGMENT AB	2.4-64
2.4-16	RELATIVE ERROR BETWEEN THE ANALYTICAL AND NUMERICALLY COMPUTED PRESSURES ALONG THE LINE SEGMENT AB	2.4-65
2.4-17	FLOW CHART ILLUSTRATING SEQUENCE OF ACTIVITIES FOR THE CROSS-HOLE PNEUMATIC AND HYDRAULIC PROTOTYPE TEST	2.4-68
2.4-18	DIAGRAM OF USGS DATA-ACQUISITION SYSTEM	2.4-71

## 1.0 INTRODUCTION

Fluid injection or withdrawal (production) field tests are used to evaluate the in situ permeability of a geologic formation subjected to natural overburden and confining stresses. Laboratory testing of core is another method commonly used to evaluate formation permeability. Unfortunately, laboratory permeability tests require subjecting the drill core to stress conditions expected in the field in order to accurately determine in situ permeabilities; this requires prior knowledge of the stress conditions including stress directions and magnitudes. In addition, the in situ permeability of fractured formations with high fracture permeability would be grossly underestimated if laboratory test results on core, which usually represent matrix permeabilities, are used exclusively.

Another alternative to measuring permeability directly from cores or in situ field tests is to use a fracture model to estimate permeability indirectly (Van Golf-Racht, 1982; Rissler, 1978; Snow, 1985). Fracture data, including fracture orientations, lengths, surface roughness, densities and apertures, are collected from drill hole video, caliper, core and geophysical logs and then used directly in a fracture model to compute formation permeability. This method is somewhat restrictive because a large fracture database is required to characterize the formation and determine permeability; there is a great deal of uncertainty associated with measuring in situ fracture aperture

Analysis of the test results is dependent upon flow domain boundary conditions, the type of fluid injected into the formation (i.e., water or gas), the saturation state of the formation, and the type of test conducted (e.g., steady state, transient, or instantaneous injection).

Single-hole fluid injection or production field tests are also commonly used to evaluate reservoir or aquifer parameters. These tests utilize only one active well and no observation wells. Formation parameters are evaluated from data (flow rates, pressures, and temperatures) collected from the single borehole. Single-well tests are often preferred over multiple-well tests because of the obvious cost-savings of drilling one hole over drilling multiple holes. From a technical standpoint, however, single-well tests cannot be used to identify flow domain boundaries, nor investigate anisotropy. In addition, cross-hole testing has the advantage of generally investigating more reservoir volume than a single-hole test (Earlougher, 1977).

Several exploratory shaft (ES) tests will utilize cross-hole tests as shown in table 2.4-1. These ES tests are designed to satisfy Department of Energy (DOE), Nuclear Regulatory Commission (NRC) and Environmental Protection Agency (EPA) regulatory issues, guidelines and technical positions; and address issues, programs, and information needs put forth in the Nevada Nuclear Waste Storage Investigations (NNWSI) Project Issues Hierarchy. The NNWSI hierarchy issues or programs pertaining to the use of cross-hole tests in the ES are also listed in table 2.4-1, and

briefly described below along with a short description on how cross-hole testing will be utilized during each ES test. Note, that only hierarchy issues applicable to cross-hole testing are described; however, other issues and information needs not addressed by cross-hole testing, but addressed by other aspects of each ES test, may apply. The NNWSI hierarchy issues hereinafter referenced in this test plan is the version dated June 23, 1987. A detailed written description, purpose and rationale for each ES test can be found in Part II, Chapter 4.0 of the NNWSI Exploratory Shaft Test Plan (ESTP).

1. Radial boreholes test: Cross-hole water injection testing will be conducted across four hydrogeologic contacts. These tests will be used to determine whether the contacts act as barriers to flow allowing perched water conditions to form. The barriers may be created by capillary action (a fine-grained layer overlying a coarse-grained layer) or by high percolation rates causing ponding on top of a low permeability layer. Lateral flow of perched water along dipping contacts could result in a preferential pathway for radionuclide migration and water flow (Montazer and Wilson, 1984). NNWSI hierarchy performance issues 1.6.1 and 1.6.3 address the need for site information and design concepts to identify the fastest paths of likely radionuclide travel and to calculate the ground-water travel time along these paths.

2. ~~Calico Hills test:~~ Cross-hole testing will be used to determine the permeability of the Ghost Dance fault if it is

effects. The excavation effects test addresses NNWSI hierarchy Issue 1.7.2; determination that the subsurface conditions encountered and the changes in those conditions during construction and waste emplacement operations, are within the limits assumed in the licensing review.

5. Infiltration test: The ES Infiltration test is designed to study water flow through a fracture network and imbibition of water into matrix blocks. Cross-hole gas injection testing will be used to characterize the fracture network (i.e., establish continuity between boreholes, and determine fracture permeabilities and apertures) before and after the introduction of water into the system. NNWSI hierarchy site program 1.13.2, description of the unsaturated zone hydrologic system at the site, also applies directly to this test.

#### 1.1 PURPOSE

The purpose of this prototype test is to develop a standard cross-hole pneumatic and hydraulic test system that can be used in the following ES hydrologic tests proposed by the U.S. Geological Survey: 1) radial boreholes test; 2) Calico Hills test; 3) bulk permeability test; 4) excavation effects test; and 5) Infiltration test. The test system is made up of several components including test hardware, software, technical procedures, data analyses, and field test configuration. Developing, testing, and refining each of these components during prototype testing will increase the likelihood that ES tests that utilize

### 1.3 OBJECTIVES

The primary objective of the pneumatic and hydraulic cross-hole prototype test is to develop and/or refine field equipment (hardware), software, technical procedures, analyses, and field test configuration. A summary of specific objectives follows:

A. Design, fabricate and test a straddle packer system for measuring in situ permeabilities as small as  $1.0E-17$  m<sup>2</sup> (0.01 mdarcy) with a confidence level of 95% (2 standard deviations).

B. Develop a field test configuration for testing a hydrogeologic contact in order to detect lateral flow along the contact. Develop methods of analyzing cross-contact tests, conduct cross-contact tests in G-tunnel, and prepare final procedures for ES contact testing.

C. Develop a field test configuration for determining the permeability of a known fault, develop methods of analyzing fault tests, conduct tests along a known fault in G-tunnel, and prepare final procedures for ES fault testing.

D. Develop analytical method of interpreting cross-hole gas injection tests for determination of the 3-dimensional gas permeability tensor, conduct cross-hole anisotropy tests in G-tunnel in support of the bulk permeability prototype test, and prepare final procedures for ES testing.

### 2.0 DESCRIPTION OF WORK

Prototype cross-hole pneumatic and hydraulic testing consists of three activities including 1) laboratory testing,

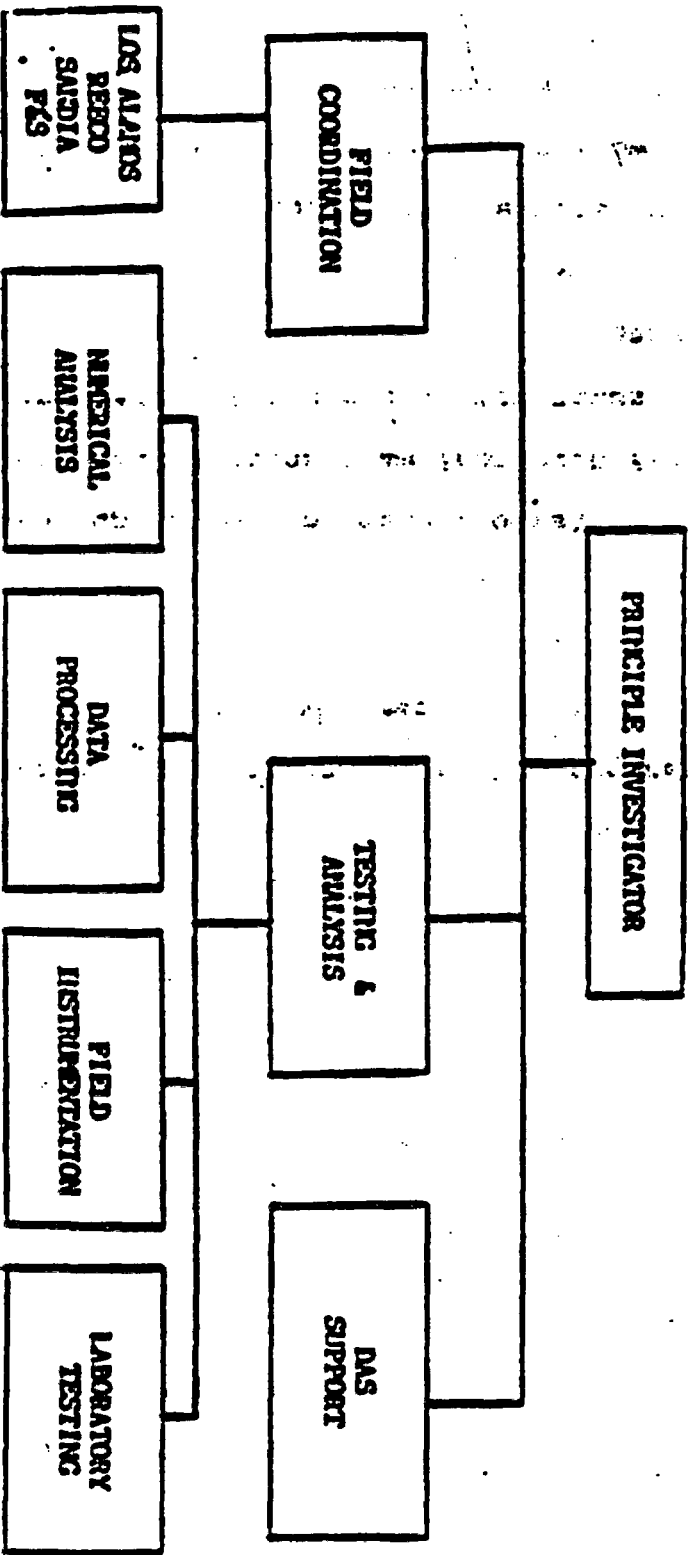


Figure 2.4-1. STAFF ORGANIZATION CHART.

communications with Roger Zimmerman).

Upon leaving the flow regulating and monitoring manifold, the fluid will flow through a flexible hose to the fluid injection (withdrawal) line. The injection line consists of a high-pressure, 1.27 cm (0.5 inch) inside diameter, thick-walled, nylon tube. The injection line extends from the collar of the hole through the packers to the test interval underground. Fluid is removed from or injected into the test interval and geologic formation via the fluid injection line.

A straddle packer system, consisting of at most four inflatable packers placed in series and separated from one another by spacer rods or well screens, will be placed in the active borehole (Figure 2.4-2). Gas or water will be injected into the test interval isolated between the second and third packers in the injection borehole. In the case of gas withdrawal, gas will be pumped from the test interval using a vacuum pump. In both cases, the pressure response caused by injection or pumping will be monitored in the test hole and in the adjacent observation borehole(s). The observation borehole(s) will also contain a straddle-packer system thus providing up to three observations zones per hole where the response from fluid injection can also be monitored. In addition to the test interval, the test borehole contains two guard zones which straddle the test interval. These zones will be used to monitor fluid leakage from the test interval past the packers straddling the test zone (past the second or third packers in Figure 2.4-2). It should be noted

that the straddle-packer system is constructed so that individual packers can be removed from the system thus making the string shorter. A shorter string may be required if the desired test interval lies close to the collar or bottom of the hole, however, it may result in the loss of one or more guard zones. Three types of sensors will be utilized for monitoring in situ fluid pressure, fluid temperature, and relative humidity in the guard and test intervals. They include strain gauge pressure transducers for measuring absolute pressures, resistance temperature devices (RTDs) for measuring temperature and thermocouple psychrometers for measuring relative humidity. Electrical leads for the sensors will be routed through the packers using gas and water tight connectors to the collar of the drill hole.

Three hydrogeologic conditions have been selected in G-Tunnel for the activities described in this prototype test program: 1) cross-contact testing will be performed between the welded unit and underlying transition unit both belonging to the Grouse Canyon member; 2) fault testing will be conducted along a known fault intersecting the zeolitized nonwelded Tunnel Bed 4 unit; and 3) fracture/matrix permeability testing will be performed on Unit B, the densely welded unit of the Grouse Canyon member. These activities simulate testing conditions to be encountered during the radial boreholes, Calico Hills, and bulk permeability ES hydrologic tests, respectively; and are described in greater detail below. These tests will be used to evaluate the performance of the experimental equipment described above and

lying layer.

Lateral flow may occur along a dipping hydrogeologic contact when a capillary barrier is present or when a coarse-grained layer overlies a fine-grained layer and the flow rate is relatively high creating perched water conditions. Lateral flow conditions may exist at Yucca Mountain or could exist if climatic conditions change. Lateral flow along a contact to a fault, such as the Ghost Dance fault, could result in a preferential pathway for water and contaminant migration.

Cross-contact testing in G-tunnel will allow examination of the concept of capillary barriers and lateral flow along contacts prior to ES testing. The test configuration and local geologic conditions at G-tunnel are illustrated in Figure 2.4-3 and the location of the proposed test is shown in Figure 2.4-4. Similar conditions, a welded unit overlying a rubble zone and partially welded to nonwelded zeolitized tuff, are expected to exist in the ES at the contact between the Topopah Springs welded unit and Calico Hills nonwelded unit. The contrast in pore size between Unit B (the densely welded, vitrified, fractured unit of the Grouse Canyon Member) and underlying rubble zone of Unit A (transition zone between Unit B and nonwelded Tunnel Bed 5), should provide an opportunity to test the concept of capillary barriers and lateral flow caused by these conditions. The contrast in pore size between the coarse-grained rubble zone (top of Unit A, Grouse Canyon member) and underlying fine-grained, partially welded tuff (middle of unit A) should provide an oppor-

2.4-19

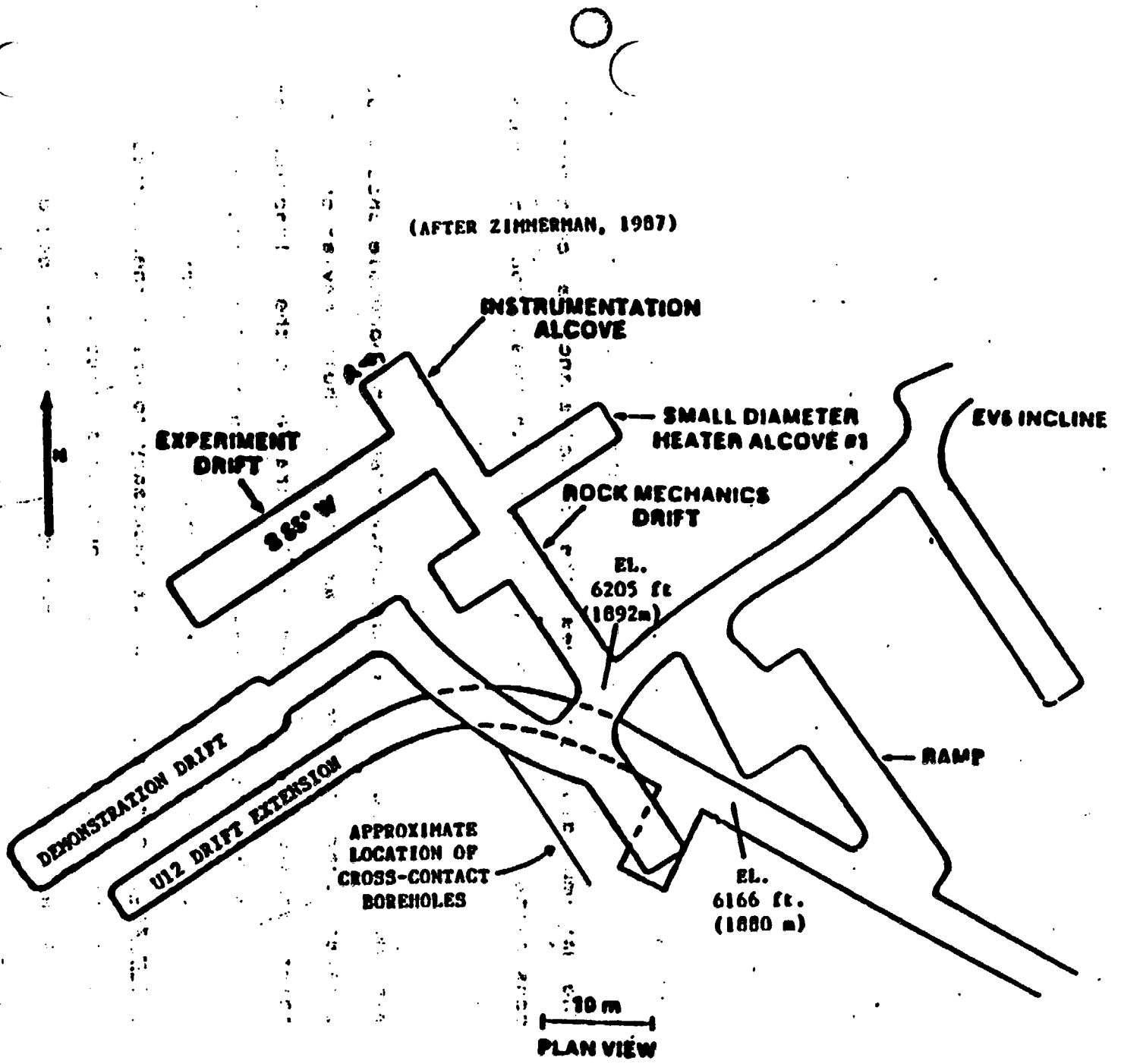


Figure 2.4-4. PLAN VIEW INDICATING THE APPROXIMATE LOCATION OF CONTACT TESTING IN THE G-TUNNEL UNDERGROUND FACILITY.

be used to determine the moisture status of the surrounding rock prior to fluid injection. The video logs will be used to view changes in lithology and locate open and closed fractures. The video logs will also be used to estimate in situ fracture apertures and determine fracture orientations. Drill cores will be logged for lithology and the following fracture characteristics: 1) fracture location; 2) type (open, closed, natural, drilling induced); 3) aperture size; 4) fill material (if present); 5) closed by homogeneous or diffused fill material; 6) fracture trace (regular, irregular, continuous or discontinuous); and 7) fracture-wall description (rugose, smooth, polished, creeping). In addition, one core sample per hole will be tested in the laboratory to determine the following hydrologic properties and functional relationships: 1) as-received volumetric water content; 2) as-received water potential; 3) porosity; 4) water saturated and gas saturated permeabilities; 5) relative permeability versus saturation; and 6) water potential versus saturation (moisture characteristic curves). This information will be used to select test intervals.

Before pneumatic or hydraulic cross-hole tests are conducted, instruments to be placed downhole (pressure transducers, thermocouples, and psychrometers) along with surface instrumentation (flow meters, pressure transducers and thermocouples) will be calibrated in the laboratory. The test tool will then be transported to G-tunnel and assembled near the collar of the hole. Leaks in the system will be detected prior

observed. The packers will then be reinflated and the observation zones monitored for an increase in pressure. In the event that no pressure response is observed, an observation zone will be positioned below and slightly down dip from the overlying injection interval. The gas will be shut-off and the injection tool pulled from the hole so the psychrometers can be removed from the system prior to water injection. The psychrometers will also be removed from the observation tool if a pneumatic connection was found.

The second stage of the second test series begins by placing the tool(s) back in the borehole(s), inflating the packers and monitoring any increase in pressure due to previous stress periods (gas injection episodes). If the pressure begins to climb the packers will be deflated and the hole will stand open until atmospheric equilibrium is reached. Again, the holes will be sealed and water injection will proceed. Water, containing a tracer, will be injected into the upper hole and the pressure response will be monitored in both the upper and lower boreholes. The reason for drilling the holes up dip parallel to the direction of dip now becomes apparent. Flow from the injection borehole to the rubble zone and along the contact is essentially a 3-dimensional problem; however, there are only two observation points, the injection and observation boreholes, which only provide a 2-dimensional look at the 3-dimensional problem. Therefore, the third observation point becomes the drift itself. Water flowing down dip from the injection borehole should inter-

2.4-25

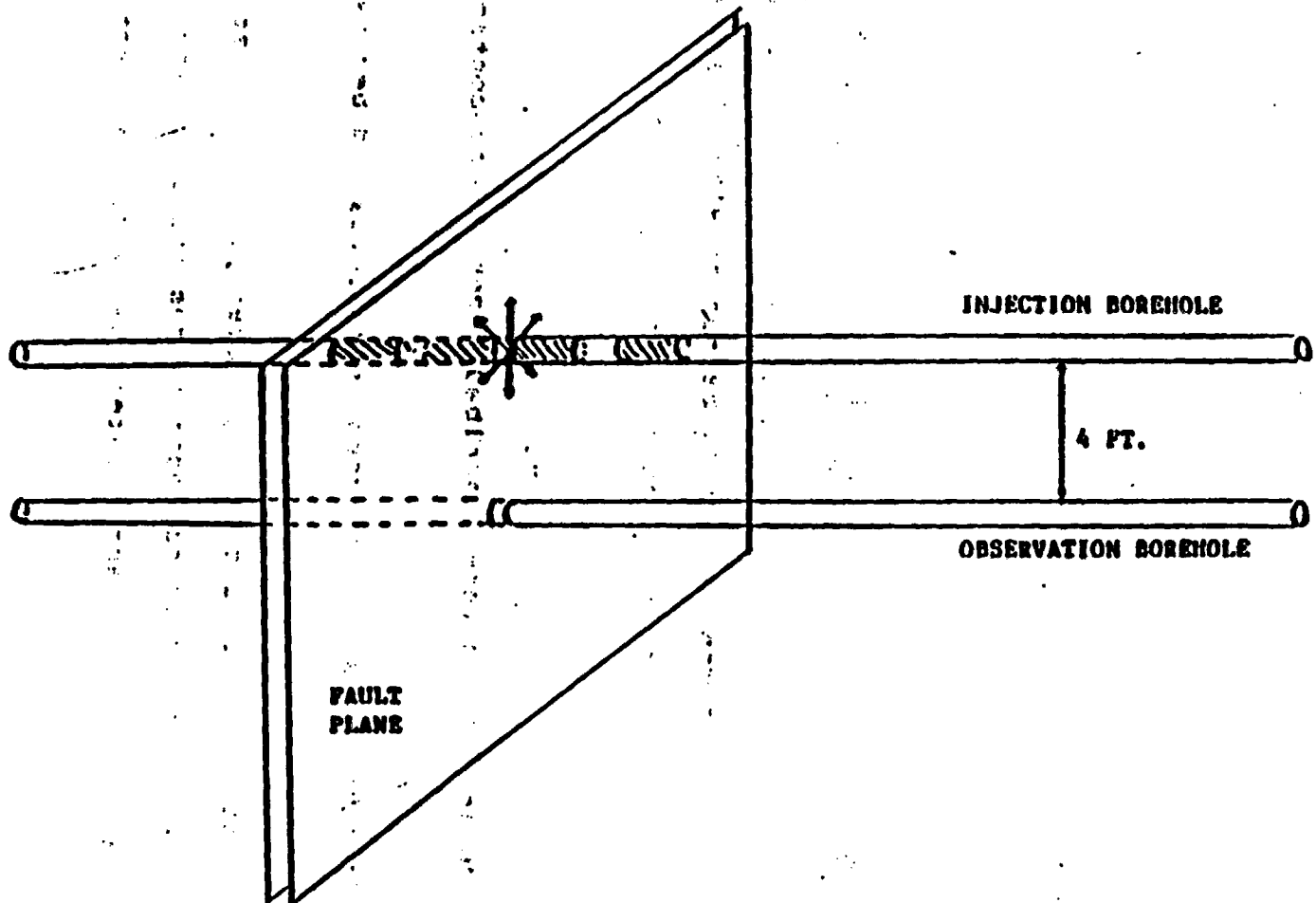


Figure 2.4-5. BOREHOLE CONFIGURATION FOR TESTING A FAULT.

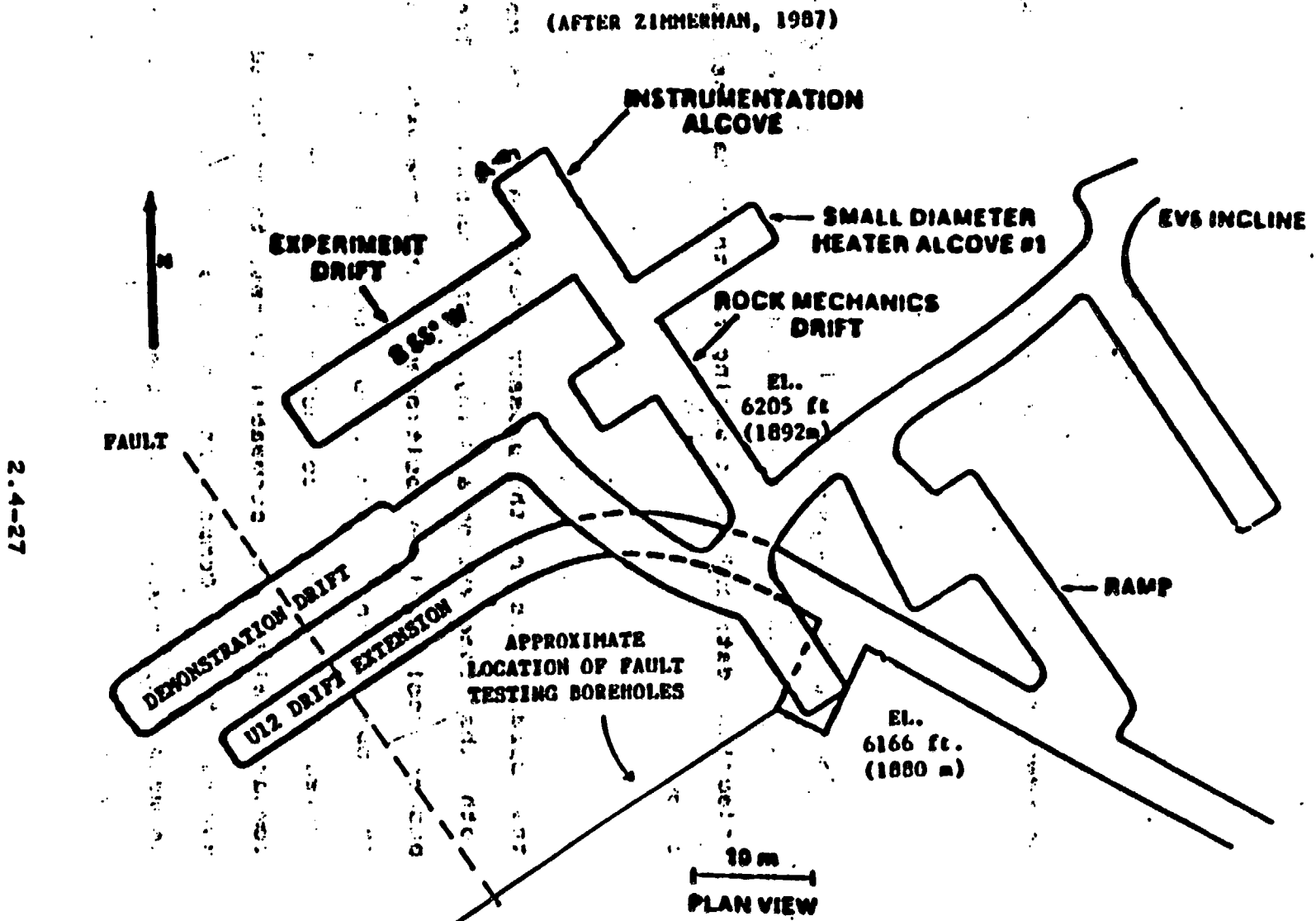


Figure 2.4-6. PLAN VIEW INDICATING THE APPROXIMATE LOCATION OF FAULT TESTING IN G-TUNNEL UNDERGROUND FACILITY.

between gas-phase and liquid-phase permeabilities measured for the same volume of rock can be obtained.

### 2.1.3 Fracture/Matrix Testing

This work is intended to support cross-hole testing needs of the Bulk Permeability prototype test. This section will describe in general terms why cross-hole testing between boreholes is important. For a detailed description of why and how cross-hole testing will be utilized in the Bulk Permeability prototype test, the reader should refer to the Bulk Permeability Detailed Test Plan.

Cross-hole tests are used to determine the radius of influence of a single-hole test. The hydrologic parameters measured using a cross-hole test are representative of a much larger volume of rock than is sampled during a single-hole test. Another very important feature of this method is it allows one to evaluate the concept of representing a fractured rock mass as an anisotropic porous medium (Hsieh and others, 1986; Snow, 1968). Cross-hole tests can be used to identify features such as faults and large conducting fractures which otherwise might go undetected using a single-hole test (Hsieh and Neuman, 1985).

Cross-hole testing will be conducted between three boreholes in GTUF during the Bulk Permeability prototype test to investigate the concept of replacing a fractured rock medium by an equivalent anisotropic porous medium. Three holes drilled parallel to the axis of the Bulk Permeability drift will be

## 2.2 EXPERIMENT PARAMETERS

### 2.2.1 Control Parameters

The control system for this prototype test consists of a low-pressure/flow regulator used to regulate the flow of gas from a high pressure gas cylinder. In addition, the flow regulating and monitoring system described in section 2.1 will be used to control the rate of flow. The pressure transducer located in the injection zone will be used to trigger the closure of a solenoid valve on the fluid injection line when pressure-pulse testing (instead of constant flow testing) is desired.

Coarse-pressure/flow adjustments are to be set manually using a pressure regulator located on the high pressure gas cylinder. A flow control needle valve, located upstream from the flow meters, will also be operated manually to provide fine flow control. The output from the flow meters will allow the operator to monitor and adjust the flow rate when desired. The control parameter is flow rate.

Pressure-pulse testing may be conducted as part of the overall testing program. A pressure-pulse test consists of injecting a slug (pulse) of gas into the test interval as quickly as possible and then monitoring the decay in pressure with time. In this case, a solenoid valve located near the injection interval would be opened and closed by the data acquisition system. The valve would open when prompted by the operator and close when the pressure in the test interval reached a user specified limit. The pressure transducer located in the test

time in hours, minutes, and seconds.

Voltages are measured for two purposes. First most, instruments must be energized in order to work. Previous G-Tunnel testing has shown that it is important to monitor, and record excitation voltages so that strange output behavior from sensors can be compared with spurious excitation voltages (R. Zimmermann, Sandia National Laboratories, 1987 G-Tunnel Facility tour). It is also important to store output voltages from sensors so that post-test recalibrations can be used to re-evaluate the data if necessary. Also, these measurements provide backups to converted measurements in case algorithms need to be checked and provide a vital backup in case the converted data are not properly recorded in the DAS.

## 2.3 OPERATIONAL AND MEASUREMENT EQUIPMENT

### 2.3.1 Operational Equipment

(a) Inflatable packers - Pneumatic type inflatable packers are to be used in the straddle-packer tool. Maximum recommended packer inflation pressures range from 1.7 to 2.0 MPa.

(b) Low-pressure flow-regulators - A low pressure regulator (pressures less than 1.0 MPa) will be used as a coarse flow rate regulator.

(c) Pressure pulse cylinder - This cylinder will be located down hole near the test interval. It will be used during pressure-pulse testing as the source for the slug or pulse of gas injected into the test interval. It has a maximum rating of

pressures.

(c) Maximum mass-flow rates for gases - Equipment is currently designed to handle flow rates of 60,000 SCCM (Standard Cubic Centimeters per Minute).

(d) Maximum volumetric flow rates of water - May exceed 40 liters/minute depending upon test-interval length and number of open fractures intersecting the interval.

(e) Maximum relative humidity - High humidities are only a problem insofar as the proper operation of the Data Acquisition System (DAS) is concerned.

#### 2.3.2.2 Sensors Required

(a) Temperature - Resistance temperature detector (RTDs) will be used to measure fluid temperature during testing. These devices operate on the simple principle that a change in electrical resistance of a wire is a function of temperature. RTDs are more accurate than thermocouples ( $\pm 0.3^\circ\text{C}$  versus  $\pm 1.0^\circ\text{C}$ , respectively) but are also somewhat fragile. Therefore, Type-T Copper-Constantan thermocouples will also be considered.

(b) Pressure - Pressure transducers are needed to operate at ambient temperatures (approx.  $20^\circ\text{C}$ ) up to pressures of 0.7 MPa in the test interval, 2.0 MPa for monitoring packer inflation, and 20.7 MPa for monitoring filling of the pressure pulse cylinder. Accuracies are dependent upon the operating range of the transducer, but readings will not vary from the true value by more than  $\pm 0.25\%$  of full scale.

Assurance (QA) Level III, calibration requirements listed in Chapter 12 of the Quality Assurance Manual (NNWSI-USGS-QMP-12.01) do not apply. Guidelines listed in Chapter 12 only apply to QA Level I and II activities. Instead, accepted industry standards or procedures will be adopted and used to calibrate prototype test instrumentation.

#### 2.4 FIELD OPERATIONS

Field preparations for each experiment discussed in section 2.1 are described below.

(a) Four diamond-drilled holes of specified depths, locations, and orientations are required for cross-hole testing (REECO). The dimensions of the holes have been specified as HQ and the length of the contact-test holes are 50 feet. The length of the fault-test holes is dependent upon the location of the drilling alcove. Holes will be located and oriented by the PI and should be drilled to within +/- 0.5 degrees of the specified directions. Three additional holes drilled parallel to the proposed bulk permeability room will also be cross-hole tested. Funding and drilling specifications for these holes will come from the bulk permeability prototype test.

(b) Water must be available at the test locations for injection into the formation.

(c) High pressure gas cylinders containing nitrogen gas should be located at the test holes during cross-hole testing. They shall be secured so that accidental puncture or valve stem

## 2.5.2 Analyses

Scoping calculations and data analyses are two very important components of this prototype test. Scoping calculations will be used to design or select equipment, design test configurations, and predict test performance prior to conducting the field test. Data analyses consist of interpreting the test data after it has been collected. Analytical and numerical techniques will be developed and used in scoping and data analysis work. These techniques will also be directly applicable to ES hydrologic tests that utilize cross-hole pneumatic and hydraulic testing.

### 2.5.2.1 Scoping Calculations

Scoping simulations are being performed to determine the maximum distance the upper borehole could lie above the densely welded unit B/rubble zone contact (Figure 2.4-3) so that lateral flow conditions will develop within 6 to 12 months after start of the water injection cross-contact test. In addition, numerical simulations are being used to predict the injection flow rates and pressures required to establish the capillary barrier. Preliminary results from 1-dimensional simulations using the finite element, unsaturated flow code UNSAT2 (Davis and Neuman, 1983), are described below. The investigators would like to gratefully acknowledge Mr. Edward Kwicklis' efforts, which included conducting the capillary barrier simulations and preparing the text provided herewith.

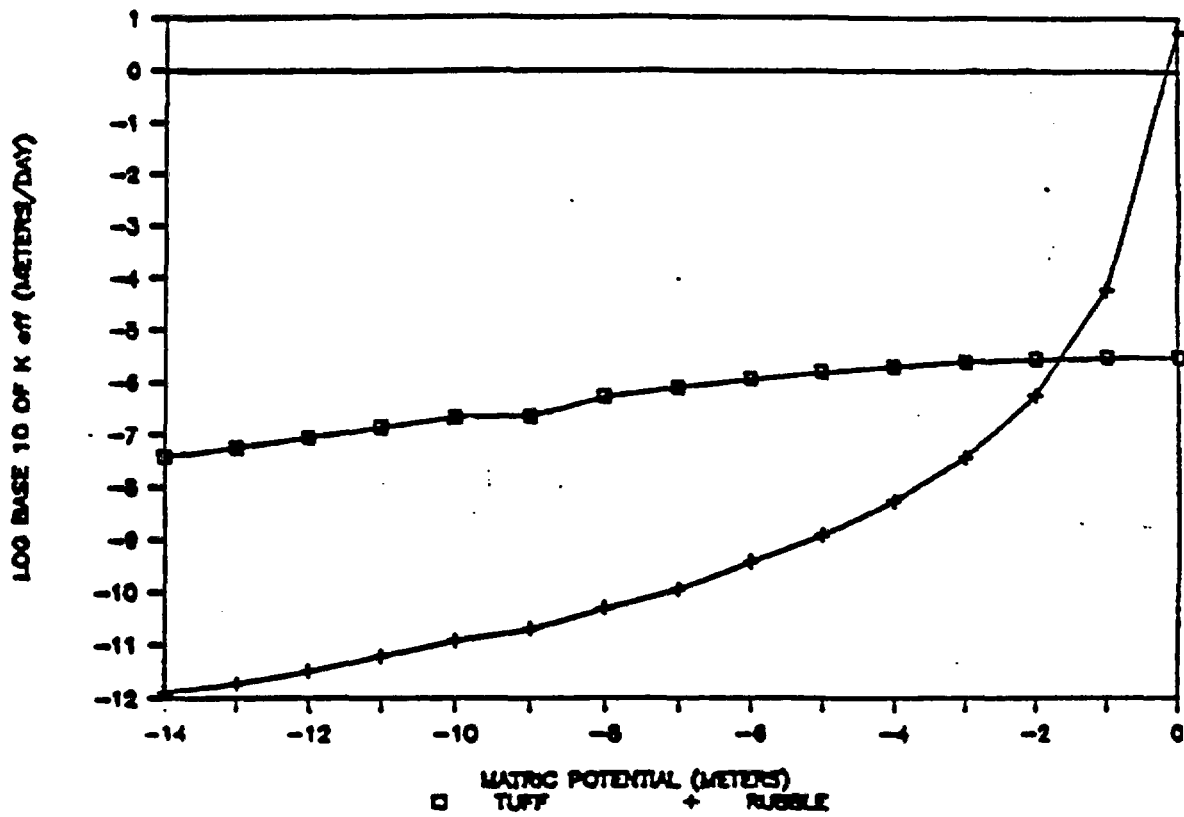


Figure 2.4-7. EFFECTIVE CONDUCTIVITY/PRESSURE HEAD CURVES USED IN 1-DIMENSIONAL SIMULATION.

than the saturated conductivity of the upper unit, thereby eliminating any chance of the capillary barrier forming; 2) when the effective conductivity in the lower layer becomes higher than the effective conductivity in the upper layer, the capillary barrier will have failed as a mechanism for retarding downward flow and inducing lateral flow along an interface. Therefore one will want to keep the pressure heads along the interface below the "cross over" point on the effective conductivity-pressure head curves. 3) Because the test must be conducted within a time frame of 6 to 12 months, the wetting front must reach the contact from the borehole (35 cm in this case), the capillary barrier must be established, and the formations response to the slowing of the wetting front must be observed at the injection borehole. The third constraint will probably not be consistent with the second constraint.

In the 1-dimensional simulations the prescribed pressure head at the upper boundary surface was increased from 0.0 to 1.0 and 10.0 meters in separate simulations. This was done in order to determine both the length of time required for the wetting front to propagate from the upper surface to the interface under different head conditions, as well as how the value chosen as the prescribed pressure affected the length of time the capillary barrier maintained its effectiveness in retarding downward flow. For the materials used in these simulations, the time at which the capillary barrier loses its effectiveness is the time at which the matric potential at the node along the interface

achieves a value greater than -1.57 meters. The changes in matric potential versus time are shown for the interface nodes in Figure 2.4-8 for each of the three cases. Note, the capillary barrier is sustained for shorter periods of time the larger the pressure head becomes at the injection boundary. This is evidenced by the time it takes the pressure head values to climb from their initial values of -11.35 meters to the "cross over" point of -1.57 meters in Figure 2.4-8.

In 1-dimensional simulations it seems possible to demonstrate the presence of a capillary barrier by monitoring how the surface-flux rate decreases with time. Figure 2.4-9 shows the decrease in the flux at one of the two nodes along the upper boundary (the location of the borehole) for two cases. In the first case, the column consists entirely of welded tuff. In the second case, the tuff overlies the rubble zone. The interface lies at a depth of 35.0 cm (1.1 ft.). For the homogeneous material, the flux declined smoothly. For the two-layer case, the initial decline in flux follows the curve for the homogeneous case; however, from approximately 130 days to 180 days into the simulation, there is a sharp decline in the surface flux. After 180 days the flux appears to have leveled off at a constant value.

Under a constant positive pressure the surface flux in a homogeneous material gradually declines and approaches a value equal to the hydraulic conductivity of the material as the total head gradient approaches unity, that is, the gradient of the

# PRESSURE HEAD CHANGE WITH TIME

AT LOCAL POINT LYING ON CONTACT

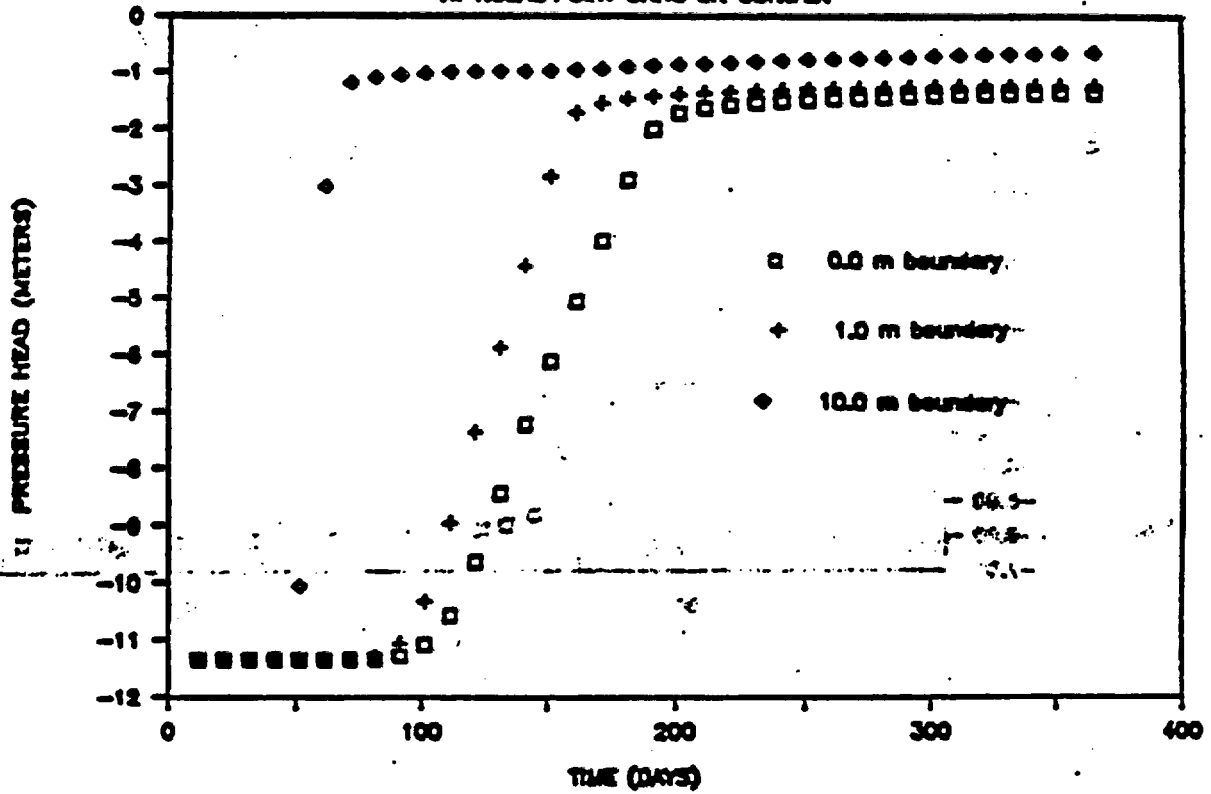


Figure 2.4-8. CHANGE IN MATRIC POTENTIAL VERSUS TIME FOR THE 0.0 M, 1.0 M, AND 10.0 M PRESSURE HEAD INJECTION SIMULATIONS.

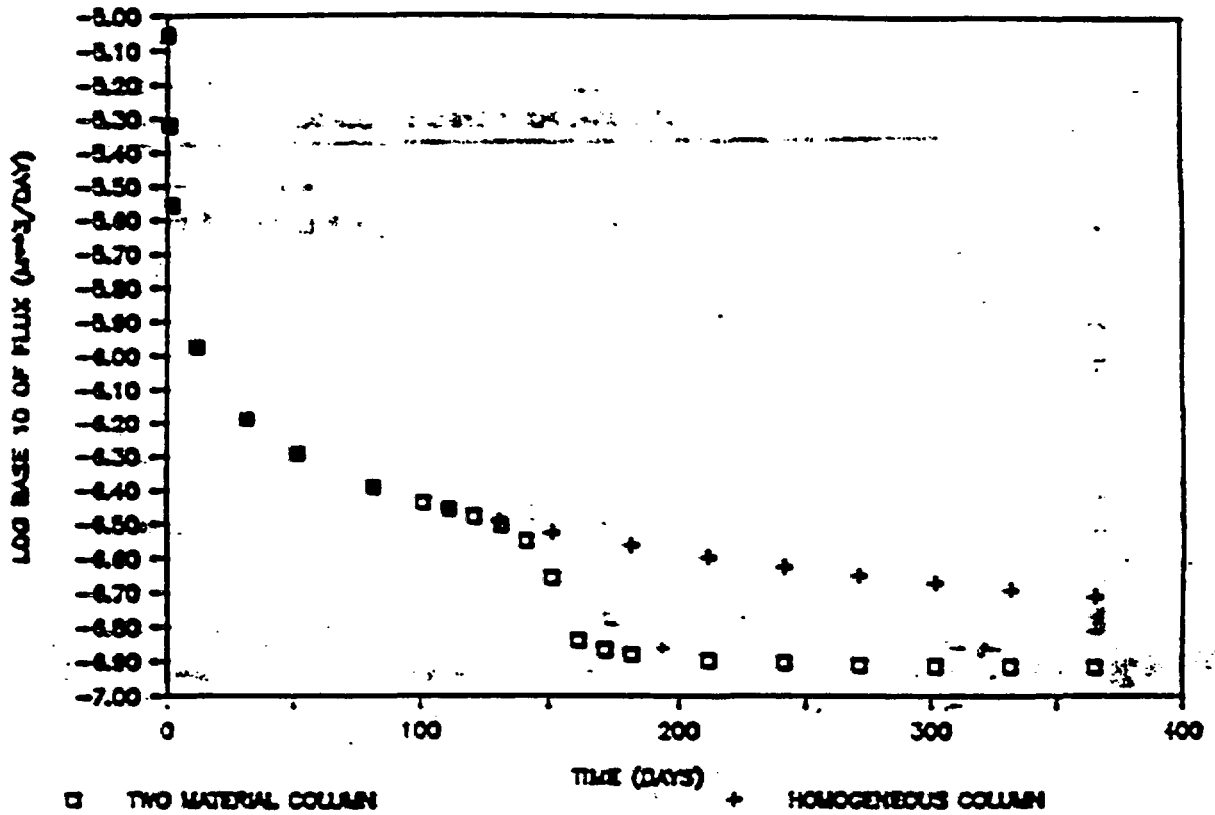


Figure 2.4-9. CHANGE IN FLUX RATES WITH TIME AT THE SURFACE BOUNDARY FOR A HOMOGENEOUS SAND AND TWO LAYER COLUMN.

FOR THE PURPOSES OF THIS REPORT, THE FLUX RATES WERE MEASURED AT THE SURFACE BOUNDARY OF THE COLUMN. THE FLUX RATES WERE MEASURED AT THE SURFACE BOUNDARY OF THE COLUMN.

matric potential becomes zero. In the two layer case the lower material is unable to transmit water away from the interface as fast as it can be delivered to the interface when the interface matric potential is less than the "cross over" potential. Hence, the moisture content and matric potential in the upper layer increase at a rate greater than that which occurs when the material is homogeneous. This causes the total gradient near the upper surface to approach unity much quicker than in the homogeneous case resulting in a reduced flux rate as indicated in Figure 2.4-8. Similar results were obtained for the cases in which the pressure was maintained at 0.0 and 10.0 meters at the upper nodes.

Based on the 1-dimensional simulations presented above, it appears that a borehole located approximately 35 cm above the contact in G-Tunnel and a constant pressure transient test analysis could be used to characterize a hydrogeologic contact. It remains to be demonstrated, however, that a similar decline in fluxes can be observed when flow is 2- or 3-dimensional, in which case lateral flow above the interface and away from the injection point is possible. 2-dimensional simulations will be conducted in future scoping work in an attempt to address this concern and to determine the range of flow rates that might be encountered in the field. This concludes the scoping work performed on capillary barriers to date; gas flow scoping simulations conducted thus far are described in detail below.

Another numerical model, DGAS2, coded and validated by R.W.

Healy of the USGS central region research branch, is being used for gas flow simulations. DGAS2 is an undocumented, block centered, finite difference, linear and axisymmetric flow code developed especially for simulating isothermal gas flow through porous media. It is being used for scoping and data analysis purposes for this QA level I, H, prototype testing activity only. The code's use in support of QA level I and II NNWSI-USGS work is strictly prohibited by NNWSI-USGS-QMP-3.03, Rev 0. In the event that it becomes desirable to use DGAS2 during ES hydrologic testing, the code will be documented and verified according to NNWSI-USGS-QMP-3.03, Rev 0.

In any event, DGAS2 was verified by comparing DGAS2 output results to experimental and numerical results obtained from a study presented in a classical paper by Bruce and others (1953). Bruce and others (1953) developed a finite difference, isothermal gas flow code. They compared their numerical solutions with the results from a laboratory study (gas depletion in a linear system) specifically designed to verify the model. They found that the difference between the numerical solution and experimentally determined data was well within the experimental error. Likewise, the match between the numerical solution from DGAS2 and Bruce and others' (1953) experimental data was also very good. Also, DGAS2 solutions for radial gas flow were in very good agreement with numerical solutions presented in graphical form in Bruce and others (1953).

Preliminary scoping calculations were performed using DGAS2.

The objective of the simulation was to determine the location of the 0 over-pressure isobar (radius of influence) with time given an injection interval of 61 cm (2 ft.), injection pressure of 304 kPa absolute (~203 kPa over-pressure), and formation gas permeability and porosity of  $5.0E-18 \text{ m}^2$  and 0.17, respectively. The permeability and porosity values specified above are based on a range of values ( $1.1E-13$  to  $6.9E-19 \text{ m}^2$  and 0.34 to 0.09) determined from laboratory analyses of Topopah Springs unfractured drill core. Gas permeability values ( $1.0E-17$  to  $5.0E-17 \text{ m}^2$ ) for the Grouse Canyon densely welded matrix also lie in this range. The Grouse Canyon permeability values were not known by the investigators during the time period in which these simulations were conducted.

Due to symmetry, only the upper half of the test interval was simulated as shown in Figure 2.4-10. The 3.7 meter wide by 2.5 meter high axisymmetric flow domain was simulated using a 3600 nodal point mesh. Gas was injected into the flow domain via 10 constant pressure nodes evenly spaced over a 30.5 cm (1 foot) interval located on the axis of the radial domain. Figure 2.4-11 indicates the horizontal location (radial direction only) of the 0 over-pressure isobar with time as the pressure front propagates away from the injection point. The pressure front reached the outer boundary of the reservoir in the horizontal direction (3.7 meters) in 1 day. This indicates that the proposed gas injection tests can be conducted in a reasonable time frame given the conditions described above and test configurations presented in

AXIS OF FLOW  
DOMAIN

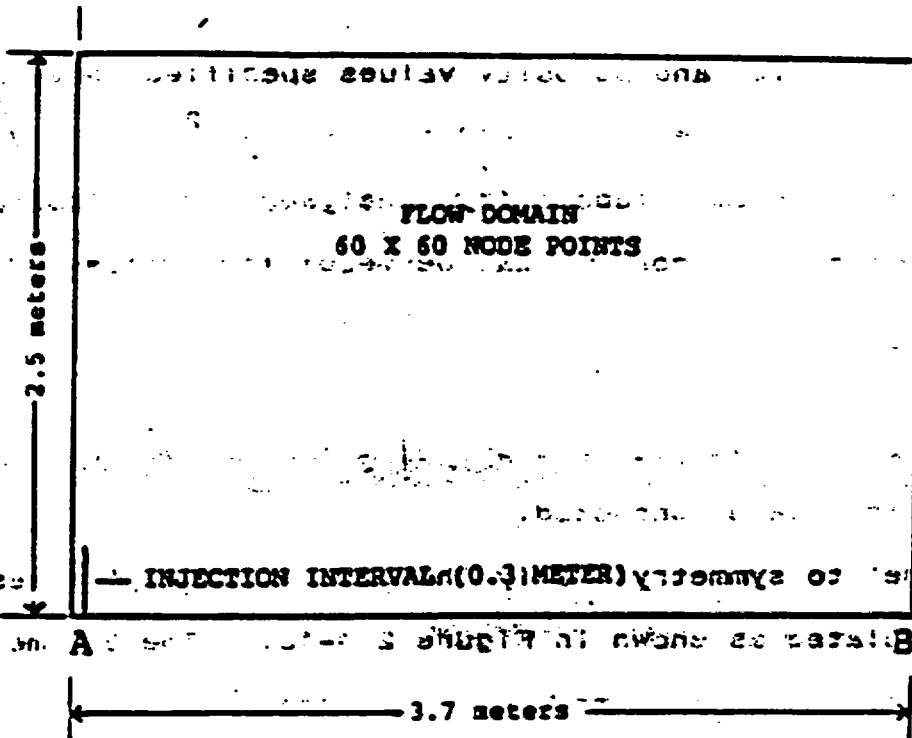
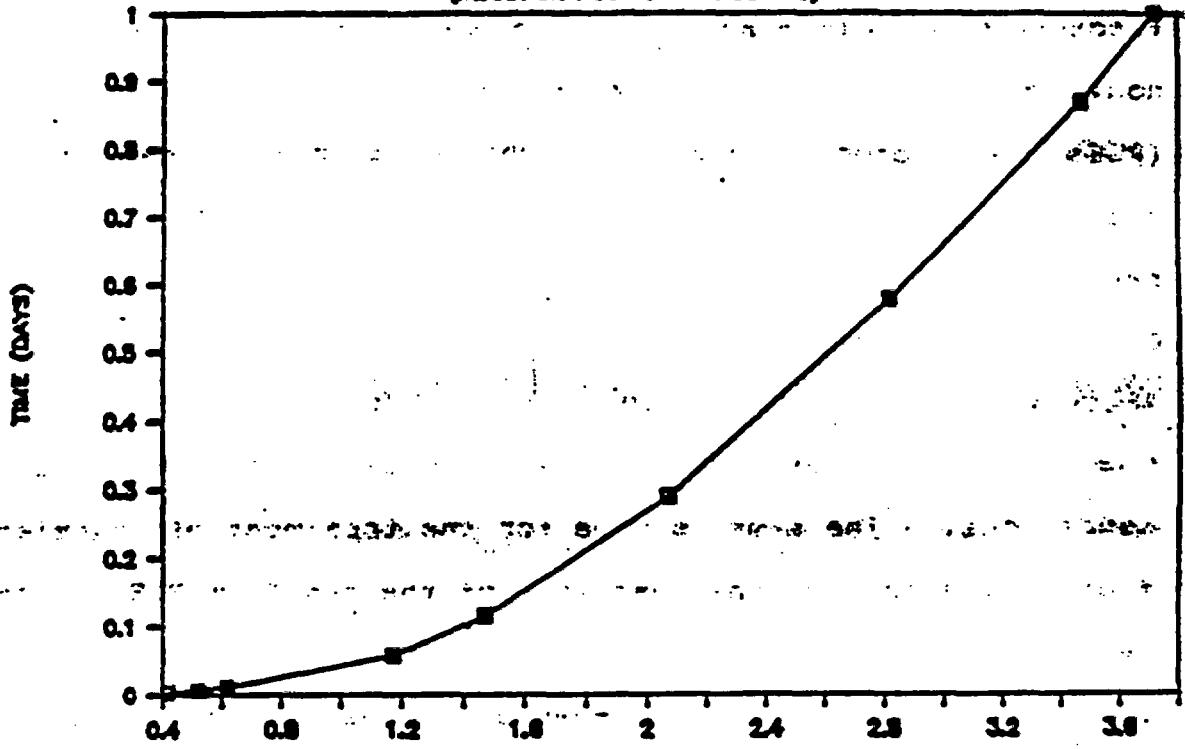


Figure 2.4-10. FLOW DOMAIN FOR GAS INJECTION SCOPING SIMULATION.

LOCATION OF 0 PRESSURE ISOBAR WITH TIME  
(INJECTION POINT AT RADIUS = 0)



radius A radius will be 0.5 radius B

of 100% is 0.5 of the radius of the well

to 100% is 0.5 of the radius of the well

radius of the well is 0.5 of the radius of the well

Figure 2.4-11. LOCATION OF THE PROPAGATING PRESSURE FRONT WITH TIME.

section 2.0.

#### 2.5.2.2 Data Analyses

Analysis of test data is complicated by several factors including complex boundary conditions such as layered media, unsaturated fluid flow (two phase flow), transient gas flow, and fracture-matrix interactions. In each case listed above, the nonlinear form of the governing partial differential equations (PDEs) and complex boundary conditions make these equations extremely difficult or impossible to solve analytically. At present, few analytical solutions to unsaturated flow PDEs exist. Oftentimes, simplifying assumptions are made in order to solve these equations (Hillel, 1971) which can result in transforming them into problems which may no longer represent true flow conditions. The same is true for the treatment of transient gas flow. Due to the nonlinear form of the gas flow PDE, it has not been possible to derive explicit solutions for general boundary and initial conditions. However, steady state analytical solutions can be readily derived for gas flow problems having various flow domain boundary configurations (see Muskat, 1937 for greater detail on this subject). Approximate methods of transient gas flow analysis have also been presented by several authors including Muskat (1937), Katz and others (1959), Rowen and Clegg (1962), Al-Hussainy and others (1968), and Earlougher (1977). An example of developmental work underway at the USGS for analyzing cross-hole gas injection tests using an approximate

method of analysis is described below. Numerical models such as TOUGH (Pruess, 1985), which can handle water, water vapor, and gas transport, or UNSAT2 (Davis and Neuman, 1983), which is an unsaturated flow model, will also be utilized extensively for data analyses.

Hsieh and Neuman (1985), and Hsieh and others (1985) developed a field method for determining the 3-dimensional hydraulic conductivity tensor and specific storage of an anisotropic porous or fractured medium. Their method utilizes cross-hole testing, that is, injecting water into (or withdrawing fluid from) packed-off sections of the active borehole and monitoring the transient response in nearby observation boreholes. An important feature of their method is it allows the investigator to determine the anisotropic nature of the medium without prior knowledge of principal hydraulic conductivity directions or magnitudes. Virtually all of the previously proposed methods required that one or more principal directions be known prior to the test (Papadopoulos, 1965; Hantush, 1966; and Snow, 1966). In Hsieh and Neuman's (1985) theoretical development begins with the continuity equation for an incompressible fluid flowing through a

fractured rock mass treated as an equivalent homogeneous, anisotropic porous medium. The governing PDE is

$$\nabla \cdot K \nabla h = S_s \frac{\partial h}{\partial t} \quad (1)$$

where  $\nabla \cdot$  and  $\nabla$  are the divergence and gradient operators, respectively;  $K$  is the hydraulic conductivity tensor;  $S_s$  is specific storage;  $t$  is time; and  $h$  is hydraulic head. Hsieh and Neuman solve this equation for the point source/point observation case, then express the analytical solution in terms of the directional hydraulic conductivity as follows:

$$\Delta h = \frac{Q [K_d]^{3/2}}{4 \pi D^{3/2}} \operatorname{erfc} \left( \frac{r^2 S_s}{4 K_d t} \right)^{1/2}$$

as  $b \rightarrow \infty$   $\operatorname{erfc}(b) \rightarrow 1$   
 as  $r \rightarrow \infty$   $\operatorname{erfc}(r) \rightarrow 0$   
 as  $k_d \rightarrow \infty$   $\operatorname{erfc}(k_d) \rightarrow 0$

where,  $\Delta h$  is the head increase at the observation point,  $Q$  is the volumetric injection rate at the point source,  $K_d$  is the directional hydraulic conductivity,  $r$  is the radius from the source to the observation point,  $\operatorname{erfc}(\cdot)$  is the complementary error function (see Carslaw and Jaeger, 1959 for a thorough treatise on the complementary error function), and  $D$  is the determinant of  $K$ . A type curve was produced so that the field data could be analyzed graphically. In turn, results from type curve matching could be used to define the hydraulic

conductivity ellipsoid from which the principal hydraulic conductivities and their directions could be computed. A similar analytical technique is being developed as part of this prototype test for the case of compressible gas flow. Data collected during the third phase of prototype testing described earlier in section 2.1.3 Fracture/Matrix Testing, will be analyzed using these techniques. Preliminary work in this area has begun for isothermal gas flow and is summarized below:

One major problem with applying Hsieh and Neuman's (1985) analysis to isothermal gas flow through a homogeneous, anisotropic medium, is the nonlinear form of the gas flow continuity equation as shown below:

$$\nabla \cdot (k \nabla p^2) = \frac{\phi \mu}{p} \frac{\partial p^2}{\partial t} \quad (3)$$

where  $k$  is the gas permeability tensor,  $p$  is the absolute pressure of the gas,  $\phi$  is the porosity of the medium, and  $\mu$  is absolute viscosity of the gas. Note that Equation (3) is in the same form as the Boussinesq Equation (if  $h$  replaced  $p$ ) which describes flow in a phreatic aquifer with a horizontal impervious base (Bear, p. 113, eq. 5-75, 1979). Equation (3) would be linear with respect to the dependent variable:  $p^2$ , if the term  $1/p$  did not appear on the right-hand-side of the PDE. One method of linearizing equation (3) is to assume that  $p = p_{ave} + p'$ ; where  $p_{ave}$  ( $\gg p'$ ) is the average pressure in the reservoir and  $p'$  is

the deviation from the average. As long as  $p'$  is small  $p_{ave}$  can be treated as a constant, thus equation (3) becomes;

$$\nabla \cdot (k \nabla p^2) = \frac{\phi \mu}{p_{ave}} \frac{\partial p^2}{\partial t} \quad (4)$$

Equation (4) is now in identical form to that of equation (1) with the gas permeability tensor,  $k$ , replacing the hydraulic conductivity tensor,  $K$ ; absolute pressure squared,  $p^2$ , taking the place of the dependent variable,  $h$ , hydraulic head; and the quantity  $\phi \mu / p_{ave}$  replacing the specific storage,  $S_s$ . Solving equation (4) yields a linearized point source/point observation solution for transient isothermal gas flow as follows:

$$\Delta p^2 = \frac{Q_m [k_d]^{\frac{1}{2}} \mu}{2\pi p_0 r (D')^{\frac{1}{2}}} \operatorname{erfc} \left( \left[ \frac{r^2 \phi \mu}{4 k_d t} \right]^{\frac{1}{2}} \right) \quad (5)$$

- where
- $\Delta p^2$  is the change in absolute pressure squared at the observation point;
  - $k_d$  is the directional gas permeability;
  - $Q_m$  is the mass flow rate of gas emitted from the point source;
  - $D'$  is the determinant of the gas permeability tensor  $k_g$ ;
  - $p_0 = MW/RT$  is the gas density;
  - $MW$  is the molecular weight of the gas;
  - $R$  is the universal gas constant;

- $T$  is the absolute temperature of the gas;
- $r$  is the radial distance from the point source to the observation point;
- $t$  is elapsed time;
- $p_{ave}$  is the average gas pressure of the reservoir;
- $\phi$  equals formation porosity;
- and  $\mu$  equals the absolute viscosity of the gas.

Equation (5) can be used to analyze gas injection test data to determine the direction and magnitude of the principal gas permeabilities and porosity of the fissured medium. In the same manner that Hsieh and others (1985) analyzed water injection test data using Equation (2) to determine the direction and magnitude of the principal hydraulic conductivities and specific storage. However, first it is necessary to determine whether the assumption that  $1/p$  can be treated as a constant holds before applying Equation (5). A test problem was set up to compare the pressure values obtained from the linearized analytical solution given by Equation (5) against pressure values obtained independently using the numerical model DGAS2.

A fictitious flow domain was created with two of the principal permeabilities directions lying in the horizontal plane and the third being normal to the horizontal plane or parallel to the vertical axis (Figure 2.4-12). The two principal permeabilities lying in the horizontal plane ( $k_1$  and  $k_2$ ) were given the same permeability values of  $10.0E-16 \text{ m}^2$ , thus permeability is isotropic with respect to the horizontal plane.

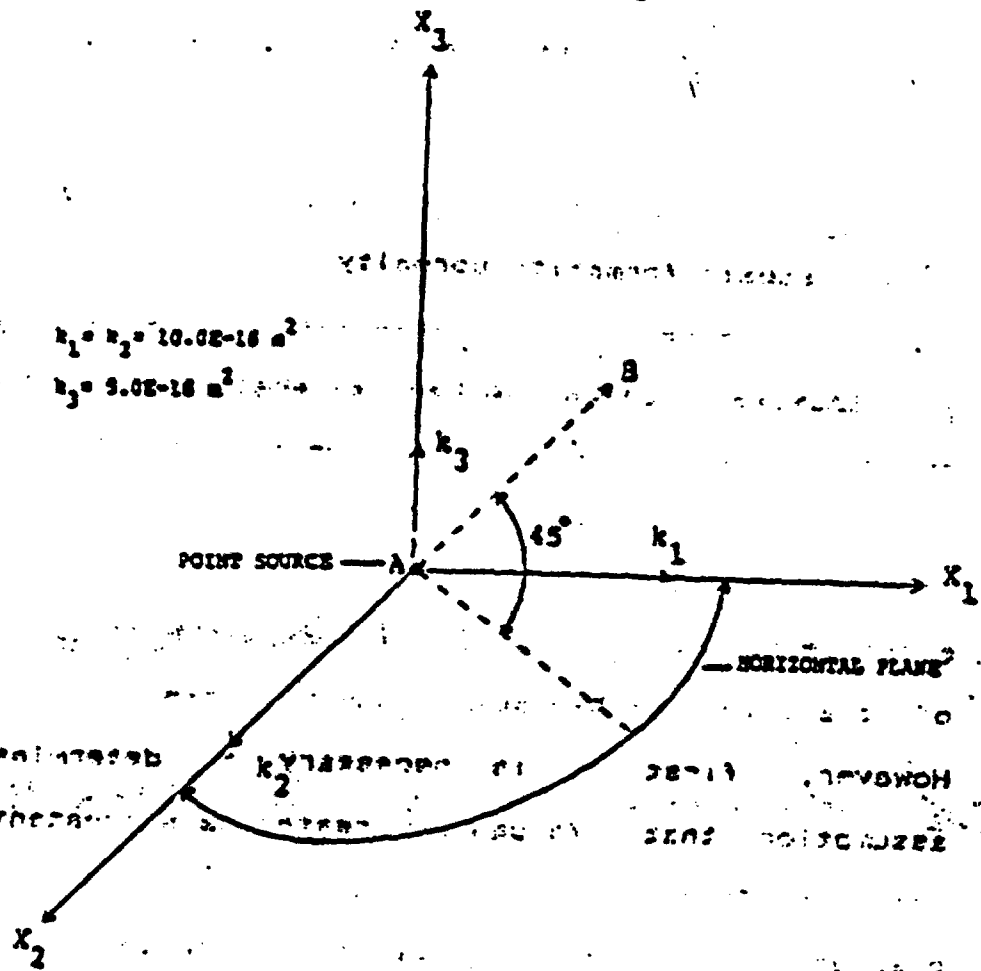


**Figure 2.4-12. ORIENTATION OF PRINCIPAL PERMEABILITY AXES WITH RESPECT TO THE POINT SOURCE AND HORIZONTAL PLANE.**

The third principal permeability ( $k_3$ ) was assigned a value of  $5.0E-16 \text{ m}^2$  or half that of the other principal permeability values. The value of the directional gas permeability ( $k_d$ ) was determined in the direction parallel to the line segment AB shown in Figure 2.4-12 using a graphical technique. The line AB begins at the origin of the axis where the point source is located and lies at an angle of  $45^\circ$  with the horizontal plane. Due to the fact that permeability is isotropic in the horizontal plane, the directional permeability in a direction parallel to any line making a  $45^\circ$  angle with the horizontal plane will always be the same. For instance, line AB could be rotated  $180^\circ$  around the vertical axis  $X_3$ , or opposite its present location in Figure 2.4-12, and the directional permeability parallel to the direction of this new line would have the same value as the old  $k_d$ .

Pressure values at various distances along the line AB were calculated using Equation (5), a  $k_d$  value of  $6.45E-16 \text{ m}^2$ , and parameter values given in Table 2.4-2. The pressure distribution is shown in Figure 2.4-13 at 600 seconds (10 minutes) after start of gas injection.  $P_{ave}$  was set equal to 101,000 Pascals (~1 atm.) which was the initial pressure of the reservoir prior to injection rather than the average reservoir pressure at 600 seconds.

Two numerical simulations having different size flow domains and grid spacings were conducted using DGAS2 which was modified to handle anisotropic flow. Input parameters into the model were

**TABLE 2.4-2. List of parameters used to generate numerical and analytical pressure distributions.**

$Q_m = 3.94E-05 \text{ kg/s} = 2000 \text{ SCCM (STD. cc/min)}$

$\mu = \text{absolute viscosity} = 1.78E-05 \text{ Pa-s}$

$k_d = \text{directional permeability} = 6.45E-16 \text{ m}^2$

$P_o = MW/RT = 1.167E-05 \text{ kg/N-m}$

$MW = \text{molecular weight of } N_2 = 28.01$

$R = \text{universal gas constant}$

$= 8.314E+03 \text{ N-m/(kgmole-K}^\circ)$

$T = \text{absolute temperature} = 288.7 \text{ }^\circ\text{K (60}^\circ)$

$k_1 = k_2 = 10.0E-16 \text{ m}^2$

$k_3 = 5.0E-16 \text{ m}^2$

$D^* = k_1 k_2 k_3 = 5.0E-46 \text{ m}^6$

$p_{\text{ave}} = 101,000 \text{ Pa}$

$\phi = \text{porosity} = 0.17$

$t = 600 \text{ seconds}$

## ANALYTICAL PRESSURE DISTRIBUTION (ALONG LINE AB)

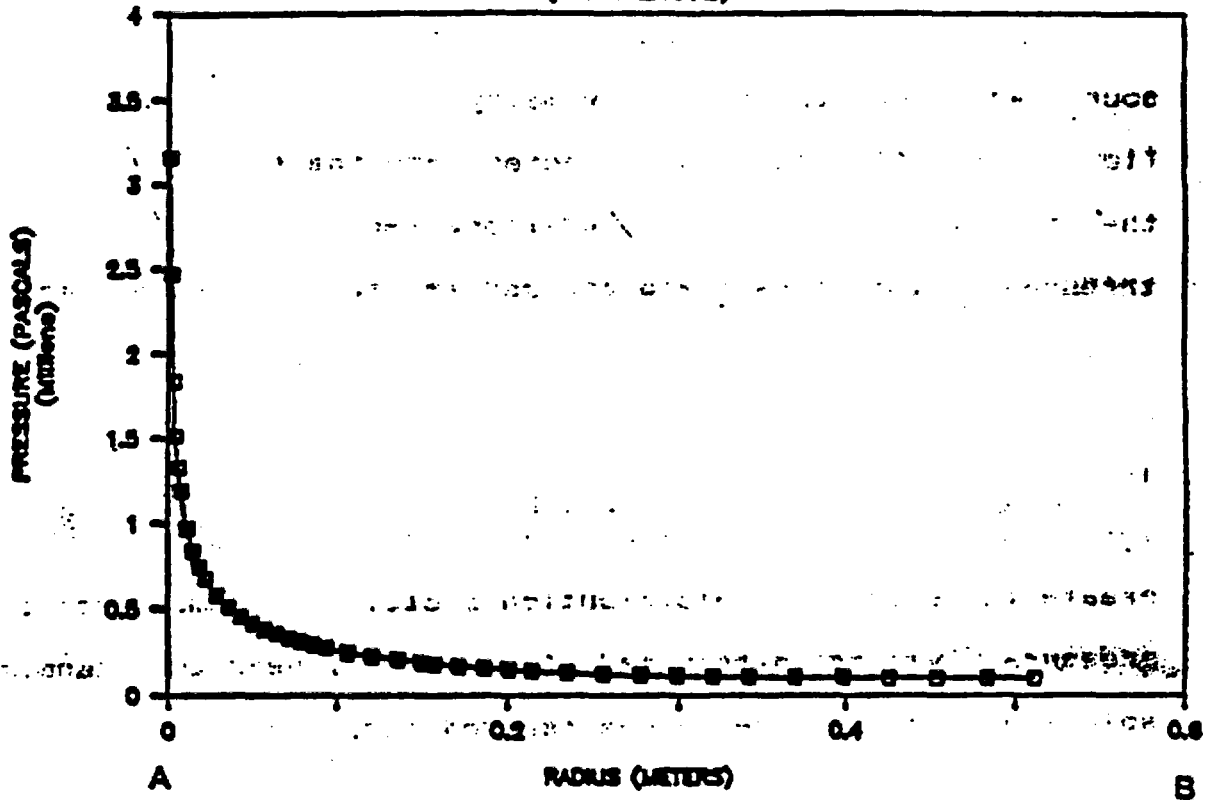


**Figure 2.4-13. ANALYTICALLY DERIVED PRESSURE DISTRIBUTION  
ALONG LINE SEGMENT AB.**

Identical to those used in the linearized analytical solution (Table 2.4-2). The point source was simulated using a single constant flow node located along the axis of the axisymmetric flow domain as shown in the vertical cross-section of Figure 2.4-14. Only the upper half of the flow domain surrounding the point source was simulated due to symmetry; in turn, only half the mass flow rate (1000 SCCM) was injected into the flow domain during the simulations. Initial conditions were set at 101,000 Pascals throughout the flow field and gas was then injected into the simulated formation. Figure 2.4-15 shows the pressure distribution that had developed after 600 seconds of gas injection for both the large and small grids. Pressure values for grid points lying on the line AB described above were used to create these pressure distribution plots. Comparison of the pressure values determined from the linearized analytical solution with pressure values derived numerically should indicate whether treating  $1/p$  as a constant was a valid assumption. Graphical comparisons of the analytical pressure values versus the numerical values for both the large and small grids are presented in Figure 2.4-16. The "error" is actually a relative error and is defined as follows:

$$\text{ERROR} = \frac{p(\text{numerical}) - p(\text{analytical})}{p(\text{analytical})} \quad (6)$$

where the pressures (p) are measured at the same radial distance

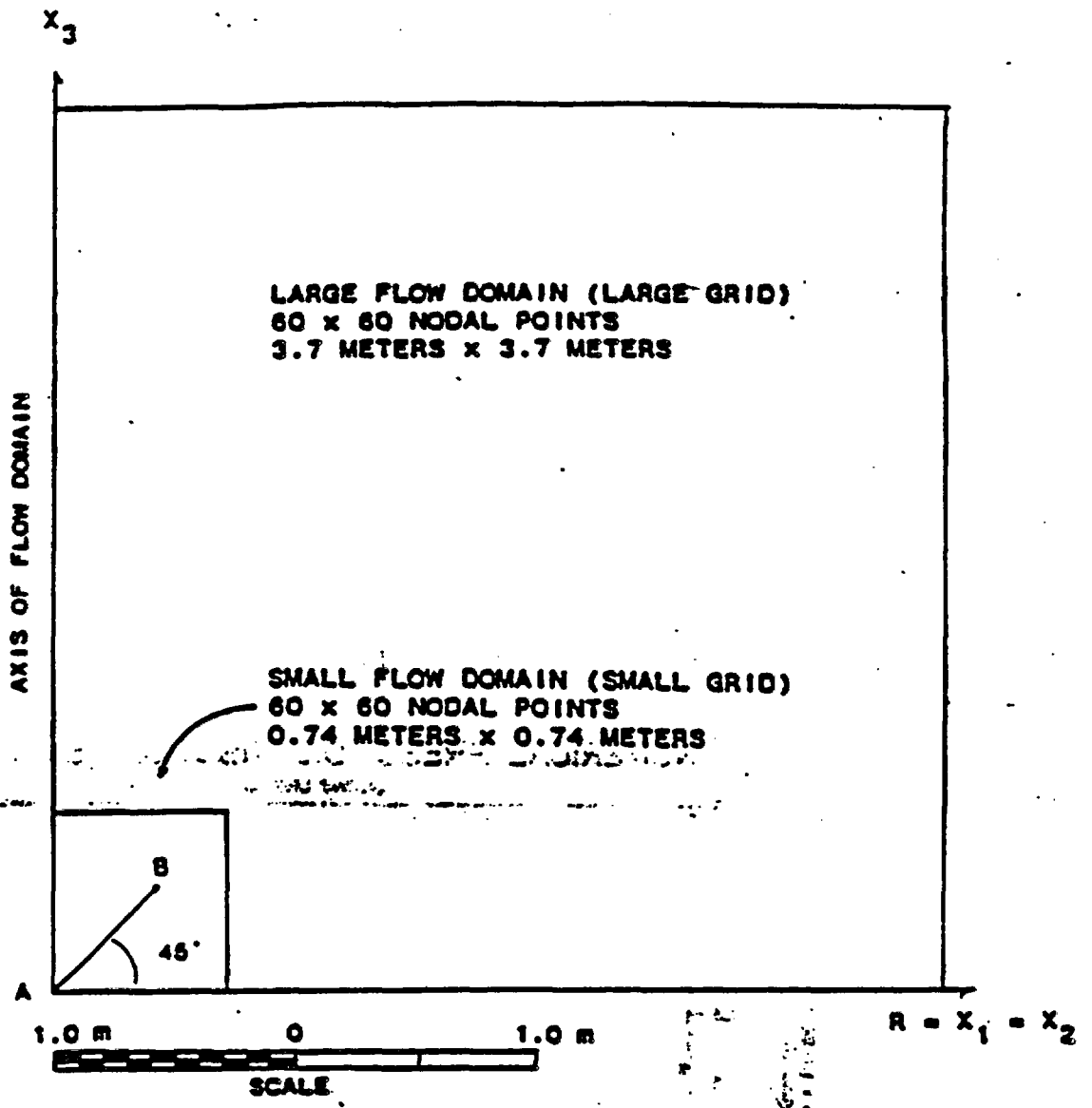
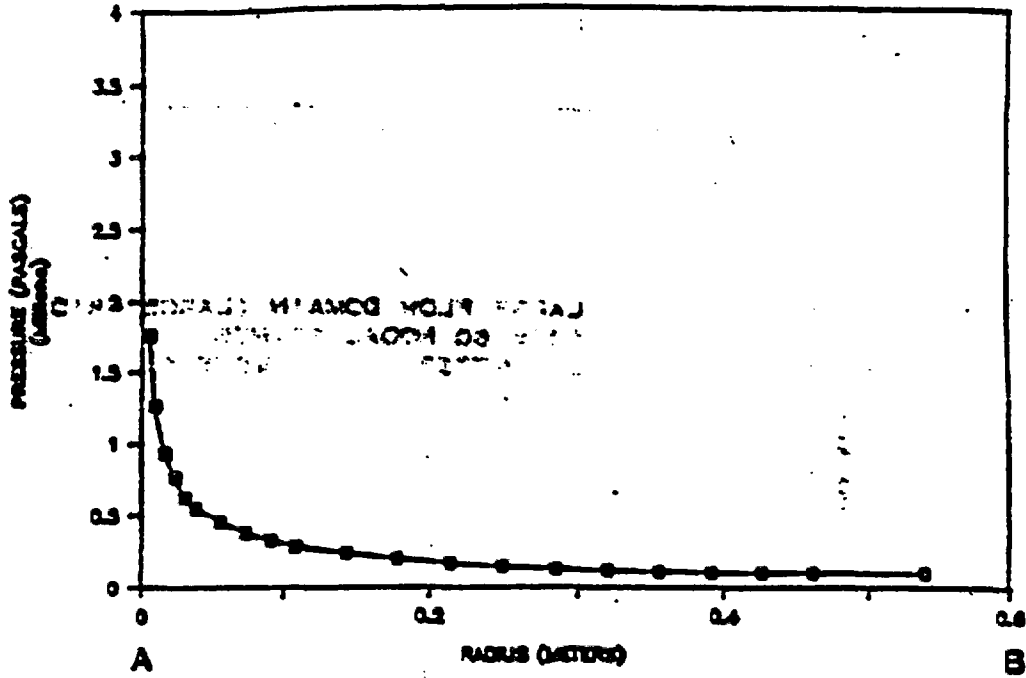


**Figure 2.4-14.** VERTICAL CROSS-SECTION THROUGH AXIS OF FLOW DOMAIN SHOWING MESH SIZE OF LARGE AND SMALL GRIDS AND LOCATION OF LINE SEGMENT AB.

NUMERICAL PRESS. DISTRIBUTION (LG GRID)  
(ALONG LINE AB)



NUMERICAL PRESS. DISTRIBUTION (SM GRID)  
(ALONG LINE AB)

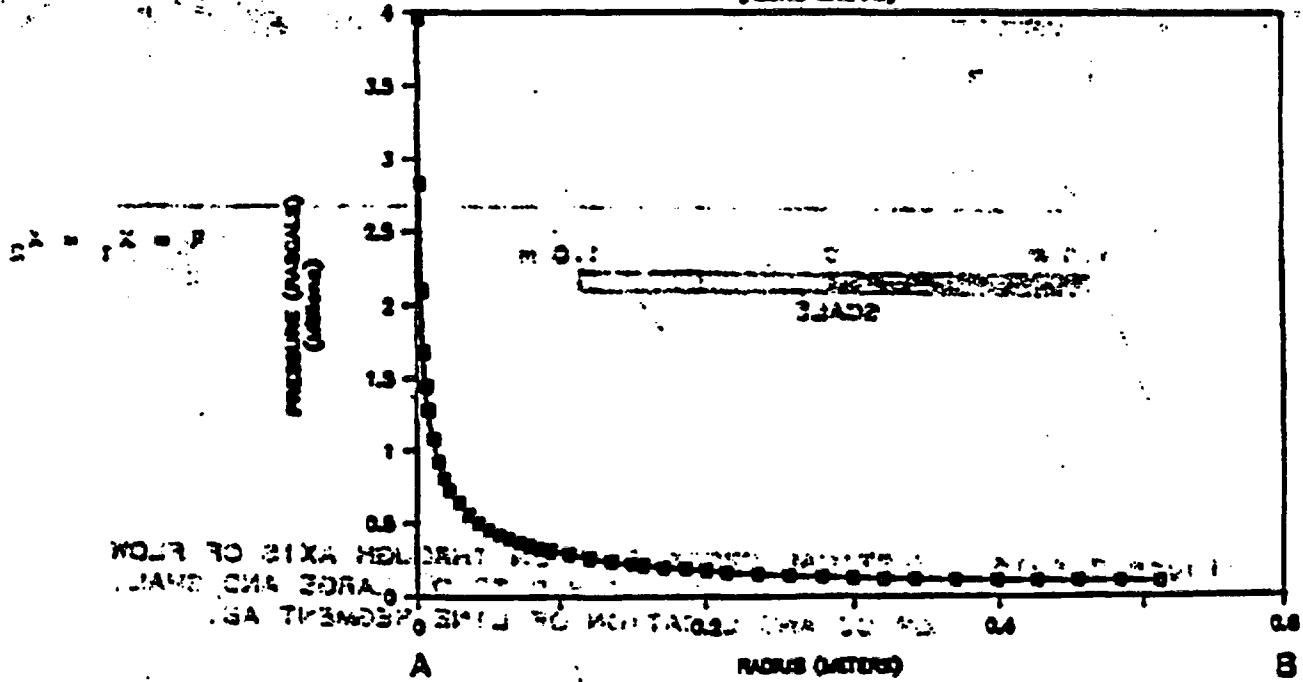
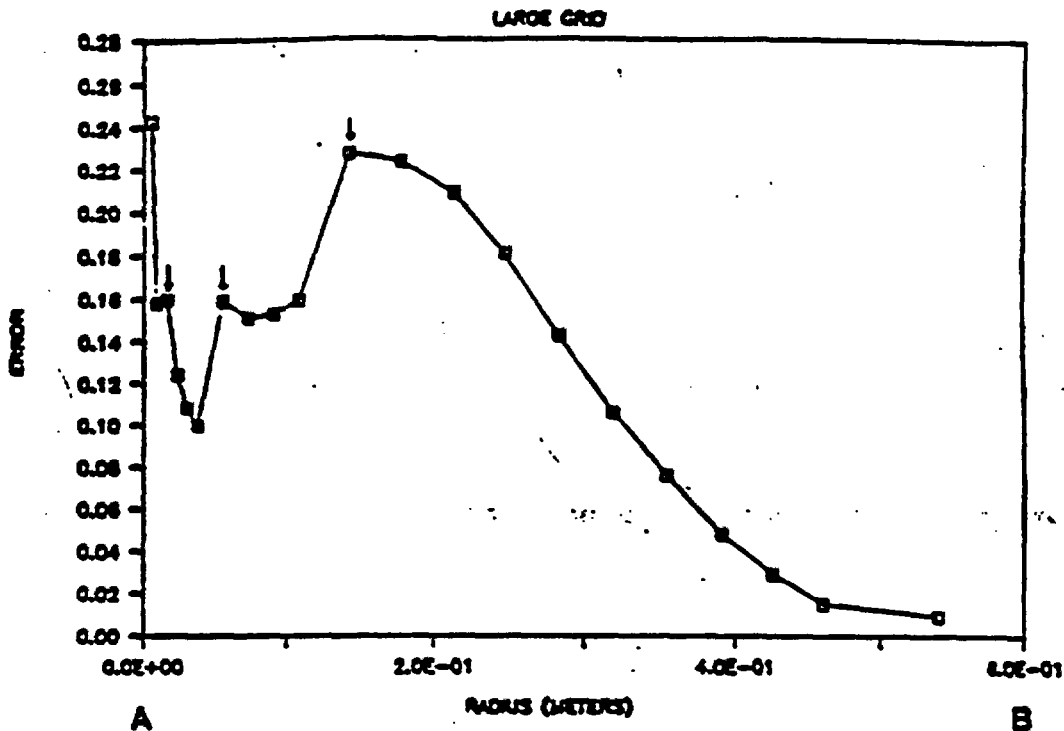


Figure 2.4-15. NUMERICALLY DERIVED PRESSURE DISTRIBUTION ALONG LINE SEGMENT AB.

### RADIAL DISTANCE VERSUS ERROR



### RADIAL DISTANCE VERSUS ERROR

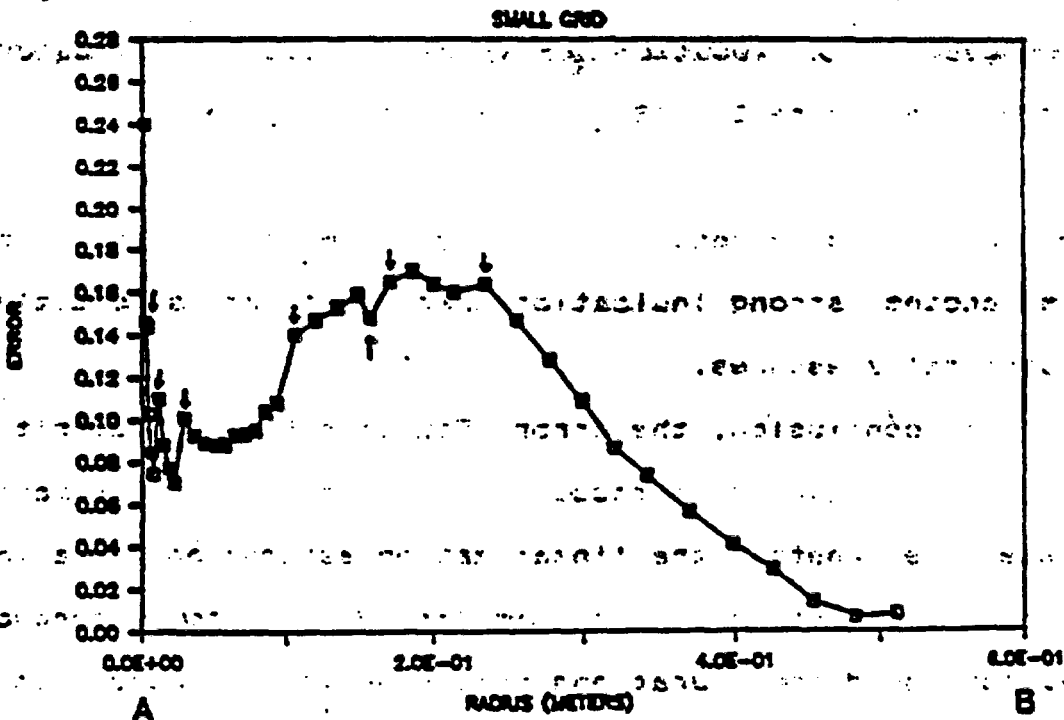


Figure 2.4-16. RELATIVE ERROR BETWEEN THE ANALYTICAL AND NUMERICALLY COMPUTED PRESSURES ALONG THE LINE SEGMENT AB.

from the point source. Intuitively, one would expect the largest errors to occur very near the point source (radius = 0 m) and become smaller further away. This is because high pressures and steep gradients near the source would easily violate the linearization assumption that the deviation in the average reservoir pressure must be small (which was set equal to the initial reservoir pressure of 101,000 Pa). Referring to Figure 2.4-18, one can see that this does indeed happen near the source, however, the errors do not drop off monotonically as expected, but rises again to another maximum at about 20 cm. This second rise in the error is believed to be a function of the grid spacing used to obtain the numerically derived pressures. This is substantiated by the fact that large changes (usually increases) in the error occur at locations where the grid spacing changes. The location of these changes are indicated by the arrows in Figure 2.4-18. In addition, the error drops from 0.23 to 0.17 for the second maximum when the small flow domain (small grid) is used instead of the large flow domain (large grid); this is another strong indication that the error is sensitive to the numerical pressures.

In conclusion, the error (Equation 6) is so sensitive to the grid spacing used in these simulations that it is impossible to determine whether the linearization assumption is valid for the parameters chosen. More simulations need to be conducted using various grid configurations before definitive conclusions can be reached. In the event that the linearization assumption is

Invalid, the steady state form of Equation (5) given below

$$\Delta p^2 = \frac{Q_w [k_d]^{3/2} \mu}{2\pi \rho_o r (D')^{3/2}} \quad (7)$$

can be used to determine the 3-dimensional permeability tensor without imposing any limiting assumptions. However, a steady state test cannot be used to determine the porosity of the fracture system, so information would be lost as a result of conducting steady state tests.

### 3.0 QA LEVEL

This work has been approved as Quality Assurance (QA) level III in accordance with NNWSI-USGS-QMP-3.02 Rev(1).

### 4.0 OPERATIONS

#### 4.1 SEQUENCE OF ACTIVITIES

Figure 2.4-17 shows a flow chart illustrating the intended sequence of activities. Activities for FY 87 and FY 88 are shown. A detailed time line gantt chart is presented in appendix A along with a short description of each activity. The time line can be used to determine activity durations, interrelationships between test activities, and approximate dates defining start and end times for activities.

Prerequisites that need to be fulfilled prior to testing include:

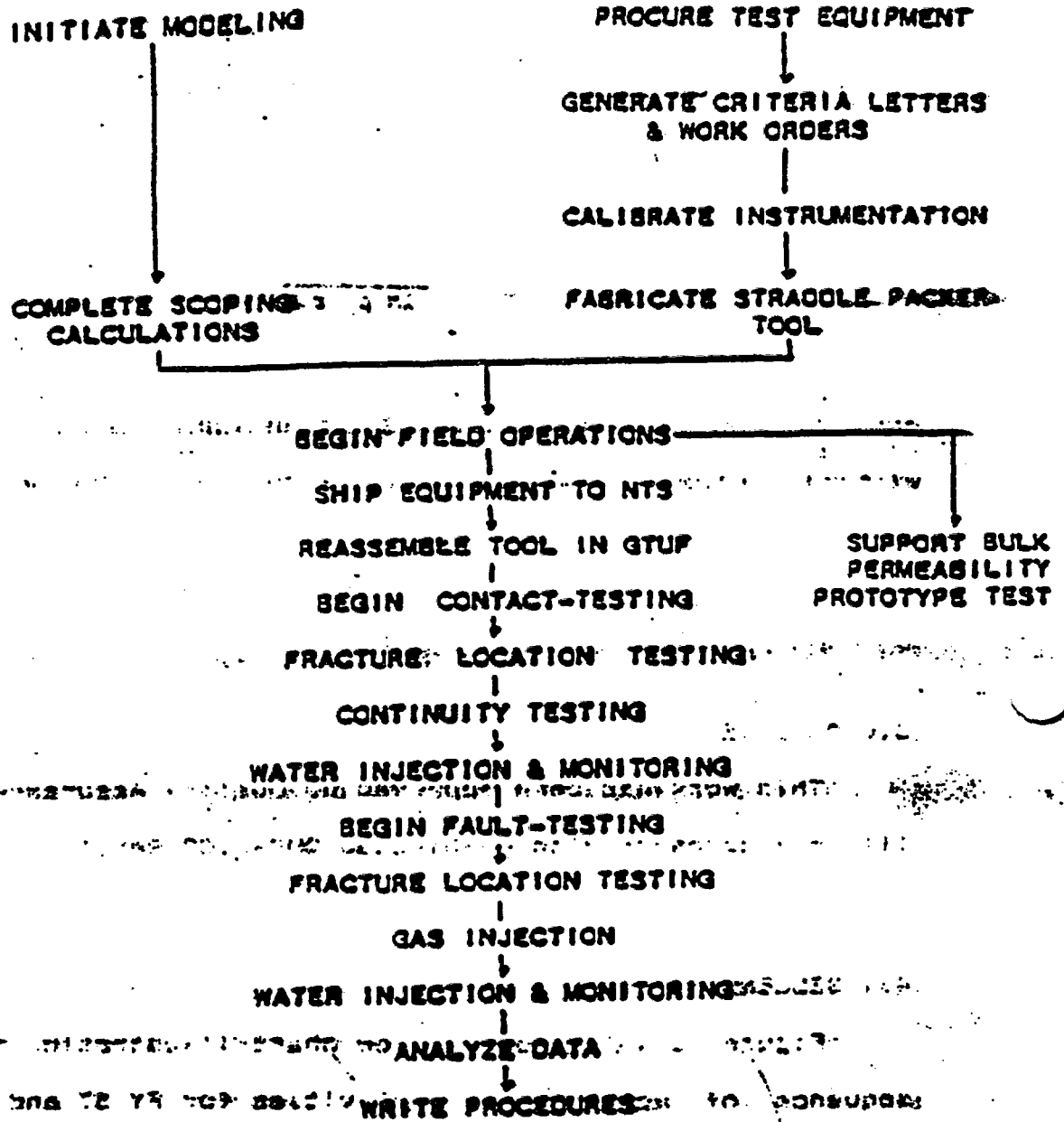


**Figure 2.4-17. FLOW CHART ILLUSTRATING SEQUENCE OF ACTIVITIES FOR THE CROSS-HOLE PNEUMATIC AND HYDRAULIC PROTOTYPE TEST.**

- (a) Complete scoping simulations;
- (b) Ordering and purchasing equipment;
- (c) Generating criteria letters and work orders;
- (d) Calibrating instrumentation in the laboratory;
- (e) Assembly and testing of the straddle packer tool in the laboratory;
- (f) Partial disassembly of the tool for shipment to the NTS G-Tunnel facility;
- (g) Reassembly of the tool underground in G-Tunnel;
- (e) Leak-detection field testing of the tool.

#### 4.2 TECHNICAL PROCEDURES

Formal technical procedures are not required for QA level III activities. However, formal technical procedures will be written as a result of activities performed during this prototype test. Data collected during prototype testing will not be used for site characterization.

Technical procedures to be developed for use in the exploratory shaft include:

- (a) Underground emplacement of packer systems in inclined boreholes.
- (b) Depth measurements from collar of borehole to straddle-packer components in inclined boreholes.
- (c) Cross-hole and single-hole water-injection test procedures.
- (d) Cross-hole and single-hole gas-injection test procedures.
- (e) Gas flow meter calibration and use.
- (f) Water flow meter calibration and use.
- (g) In situ gas-tracer test procedures.
- (h) In situ water-tracer test procedures.
- (i) Procedure for testing a hydrogeologic contact.
- (j) Procedure for testing a known fault.
- (k) Procedure for conducting a cross-hole test for determining the anisotropic permeability tensor.

Procedures that are applicable to this prototype test and currently available for use are listed in Appendix B:

#### 4.3 CHANGES IN EXPERIMENTAL PROCEDURES

Does not apply to QA Level III activities.

#### 5.0 DATA ACQUISITION SYSTEM

##### 5.1 DATA ACQUISITION SYSTEM DESCRIPTION

###### 5.1.1 Block Diagram

Figure 2.4-18 is a block diagram showing major components of the Data Acquisition System (DAS). There are two major subsystems: a DAS will be located in G-Tunnel near the experiments and Control-and-Storage subsystem outside the tunnel. The two subsystems communicate with each other by means of a duplex synchronous link with a speed of 19.2 k bps. This configuration serves as a simplified prototype for the Integrated Data Acquisition System (IDAS) that the USGS plans to use for unsaturated zone borehole monitoring at Yucca Mountain. It is also an approximate prototype for the configuration presently planned for the Exploratory Shaft Integrated Data System (IDS), and can be used to test most software and conceptual development for either of those systems.

###### 5.1.2 Hardware for the Data-Acquisition Subsystem

Some of this hardware can be reclaimed from equipment used in earlier prototype studies for the Exploratory Shaft IDS. Much of the hardware planned for use in this system was originally purchased for the Unsaturated-Zone Borehole Monitoring IDAS. If this prototype test proves out the preliminary design for the IDAS, most of the hardware "borrowed" from the Yucca Mountain

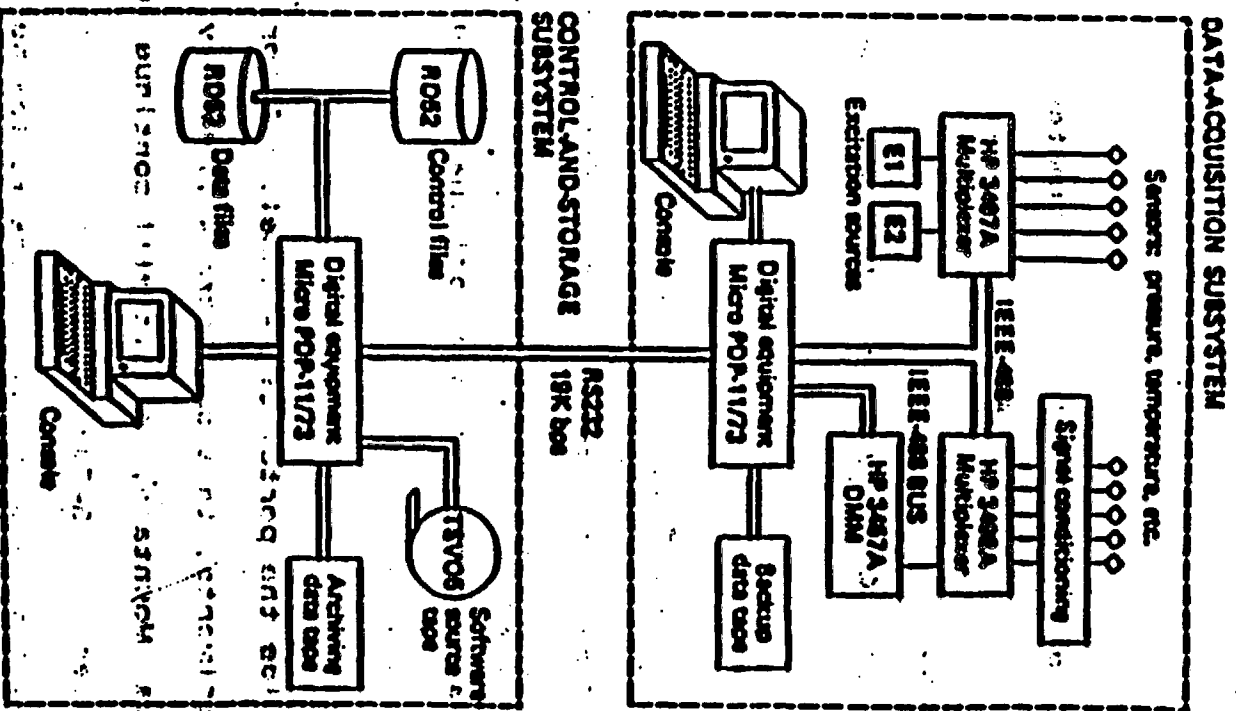


Figure 2.4-18. DIAGRAM OF USGS DATA-ACQUISITION SYSTEM

IDAS will have to be replaced with new equipment. The following equipment is planned for use in the DAS:

(a) Micro PDP-11/73 controller with CRT console, DMV-11 synchronous interface, IEEE-488 bus interface, and non-volatile CMOS memory;

(b) HP 3457A digital multimeter;

(c) HP 3497A scanner with integral DVM and several HP 3498A expanders;

(d) Qualogy DS-201 (or equivalent) sealed cartridge-tape drive for on-site data backup;

(e) Cabinet with fans, filters, UPS power conditioning and wiring panels.

### 5.1.3 Hardware for the Control-and-Storage Subsystem

All of the hardware planned for use in the Control and Storage Subsystem was originally purchased for use in the Unsaturated-Zone Borehole Monitoring IDAS. It is planned that this equipment be initially located in a protected environment outside the portal of G-Tunnel. Before beginning Yucca Mountain experiments, this subsystem will be moved to a USGS facility near Yucca Mountain, but it will continue to service the prototype studies in G-Tunnel by means of a longer datalink between this subsystem and the DAS. The following equipment is planned for use in this system:

(a) MicroPDP-11/73 computer with console and DMV-11 synchronous interface;

- (b) Dual floppy disk drive and two RD52A hard disk drives;
- (c) TSV05 1600 bpi ANSI tape drive;
- (d) Cartridge tape drives for reading backup tapes and archiving data;
- (e) WWV standard time receiver.

#### 5.1.4 Software

The programming language for this system will be transparent to the experimenter. A series of menu driven routines, operating on the Control-and-Storage computer, will guide the experimenter through assignment of A/D and excitation channels, choices of signal conditioning, timing, and excitation parameters. The software will assign labels to all readings to avoid conflicts with labels for other experiments. The labels will include cross references to appropriate calibration data, according to information supplied by the experimenter. The software will force a simulated run for each new test before the test parameters can be down-line loaded to the DAS.

Terminals at the experiment sites in G-Tunnel will permit real-time displays and interactive experiment management, but all commands for modifying an experiment are routed through the Control-and-Storage computer, which checks for authorization and conflicts before passing the commands to the DAS.

#### 5.1.5 Software Validation

Software for this system is validated by a structured programming approach. Logical requirements for software are

structured and tested before code is written; code, when written, is then tested against the predefined logic.

Software implementation is tested by simulated data-acquisition experiments that run on the Control-and-storage system. A software routine for hardware set-up allows testing of sensor wiring before data acquisition.

## 5.2 DATA COLLECTION

### 5.2.1 Data Collection Rate

The maximum rate at which this system can collect, process, and store readings is approximately 7000 readings per hour, where an average reading consists of about 5 subsamples. Each individual test collects data at a rate appropriate to the scale of measurement, subject to this overall system constraint.

### 5.2.2 Data Conversion

Data are stored in both raw form as output by the digital multimeter and in scaled and converted form. The scaling factors and equations are referenced in the data labels. Menu-driven routines assist the experimenter in selecting conversion equations appropriate to each sensor.

## 6.0 PERSONNEL QUALIFICATIONS

Quality level III work does not require formal certification of project personnel; nevertheless, the personnel involved in this testing activity could be shown to have the appropriate technical expertise.

## 7.0 NONCONFORMANCE ACTIONS

Nonconformance of Quality Level III items or processes will be documented per the requirements of NNWSI-USGS-QMP-10.01, Rev(1). Corrective action will be documented per the requirements of NNWSI-USGS-QMP-16.01, Rev(1).

## 8.0 DOCUMENTATION

As described in NNWSI-USGS-QMP-3.02, Rev(1), existing USGS good scientific practice requirements shall apply to Quality Level III work. Therefore, field notes, log books, and data records (computerized or otherwise) will be maintained with the utmost of care and precision. All manual data entries are to be recorded in permanent ink, and are to be signed and dated by the person responsible for the data collected. Computer-stored data are to be tagged, as described in Section 5.1.4 and 5.2.2. All log books and records are to be permanently maintained and archived in the USGS Denver offices. A USGS data-records management system will be maintained in Denver for support of all data collection activities associated with the USGS prototype testing program.

## 9.0 SAFETY

There are three potential hazards associated with cross-hole pneumatic testing. They include the use of high-pressure gas cylinders, high-pressure inflatable gas packers and tracers. Hazards associated with transporting and storing gas cylinders include accidental rupture of the metal cylinder or valve stem

breakage . In order to minimize this hazard the cylinders should be secured to a wall or other heavy object out of the way of operating machinery. The cylinders should be capped at all times except when utilized for testing.

The second hazard may result from exceeding the recommended inflation pressure of the pneumatic packers or from a rupture resulting from a damaged packer gland. Frequent inspection of the packer glands after each test and making sure that field crews are familiar with the manufacturer's safe operating range of the packers should help eliminate these health hazards.

A third hazard may result from the improper use of tracers.

The tracers that will be used during this prototype test will consist of nonvolatile chemicals that will be added to the test water. Taking the solution orally, absorption through the skin or splashing the tracer into the eyes present the most likely hazards. The use of proper clothing (rubber gloves and goggles) and instruction on tracer use should minimize these hazards to field personnel.

In addition, safety requirements and regulations established by Reeco and Sandia National Laboratories for G-Tunnel will be adhered to by all personnel while working in the facility.

## 10.0 REPORTS

### 10.1 PRELIMINARY REPORTS

There will be a series of administrative reports of preliminary results prepared as soon as possible after completion

of portions of the test. These administrative reports will be provided to the Department of Energy (DOE) and other related Principal Investigators from Los Alamos National Laboratory. The cross-hole pneumatic and hydraulic test system consisting of hardware, software, technical procedures, methods of data analyses, and final field test configurations will be ready for use in the Exploratory Shaft on or prior to the current expected shaft start in early spring of 1989. The time table for delivering the test system and preliminary reports, which is considered a milestone, is shown on the Gantt chart in Appendix A and designated by the task code DREPORT.

## 10.2 FINAL REPORT

The final report, to be prepared as soon as possible after completion of the test, will consist of complete data analyses and interpretation of data collected during G-Tunnel testing. It will be in the form of a paper published by the Water Resources Division of the U.S. Geological Survey. In addition, a manual or series of manuals on techniques describing procedures for planning and executing specialized work in water-resources investigations, will hopefully be published as Techniques of Water-Resources Investigations of the USGS. The time table for delivering these final reports, which is considered a milestone, is shown on the Gantt chart in Appendix A and designated by the task code DFRPT. This milestone is scheduled to be reached no later than April of 1990.

## 11.0 DEFINITIONS

A. **Prototype testing** - Exploratory shaft preparation work conducted under WBS: 1.2.8.9.4. Prototype testing involves preparing and conducting experiments, tests and field trials of proposed ES tests to validate concepts, equipment, and designs, and to develop technical procedures.

B. **Cross-hole pneumatic test** - A gas injection or withdrawal test conducted between two or more adjacent boreholes, used to evaluate rock formation parameters such as gas permeability.

C. **Cross-hole hydraulic test** - A water injection test conducted between two or more adjacent boreholes used to evaluate rock formation parameters such as water permeability or hydraulic conductivity.

D. **Measurement Equipment** - Sensors and related data acquisition system used to measure and record the physical state of a substance (e.g. temperature of a gas)

E. **Operational Equipment** - Control/feedback system used to regulate the operation of an instrument or entire experiment.

F. **Experiment** - Performance of operations that are carried out to establish characteristics or values not known previously.

G. **Test** - Process of exposing an item of hardware or physical system to a given stimulus or operational sequence to determine its acceptability or response, respectively.

H. **Analyses** - calculations or other evaluations needed to assess site characteristics, support design activities, or to support experiment designs and evaluations.

## 12.0 REFERENCES

### 12.1 PROGRAM REFERENCES

Quality Assurance Manual, U.S. Geological Survey, Nevada Nuclear Waste Storage Investigations, Oct. 27, 1986:

1) NNWSI-USGS-QMP-3.02 Chapter 3 - Design (Site Investigation Control), Section 2 - USGS QA Levels Assignment (QALA).

2) NNWSI-USGS-QMP-10.01 Chapter 10 - Inspection (Surveillance), Section 1 - Surveillance Procedure.

3) NNWSI-USGS-QMP-12.01 Chapter 12 - Control of Measuring and Test Equipment, Section 1 - Instrument Calibration.

4) NNWSI-USGS-QMP-16.01 Chapter 16 - Corrective action, Section 1 - Control for Corrective Action Procedure.

Nevada Nuclear Waste Storage Investigation, Issues, Information Needs, Studies, and Activities, unpublished document, revision date June 23, 1987.

NNWSI Exploratory Shaft Test Plan, revision 1, August 1985; edited January 1986, document control No. 28.

### 12.2 TECHNICAL REFERENCES

Al-Hussainy, R., and Ramey, H.J., Jr., May 1966, The Flow of Real Gases Through Porous Media, Journal of Petroleum Technology, p. 624-636.

Bear, J., 1979, Hydraulics of Groundwater, McGraw-Hill Series in Water Resources and Environmental Engineering, McGraw-Hill Inc.

Brooks, R.H., and Corey, A.T., June 1968, Properties of Porous Media Affecting Fluid Flow, Journal of the Irrigation and Drainage Division ASCE, 92(IR2), p. 61-88.

Bruce, G.H., Peaceman, D.W., Rachford, H.H., Jr., and Rice, J.D., 1953, Calculations of Unsteady-State Gas Flow Through Porous Media, Trans., AIME, 198, p. 79-92.

Carslaw, H.S. and Jaeger, J.C., 1959, Conduction of Heat in Solids, Oxford University Press, second edition.

Davis, L.A. and Neuman, S.P., 1983, Documentation and User's Guide: UNSAT2 - Variably Saturated Flow Model, Final Report, prepared for U.S. Nuclear Regulatory Commission, NUREG/CR-3390.

WWL/TM-1791-1.

Earlougher, R.C., Jr., 1977, Advances in Well Test Analysis, Society of Petroleum Engineers of AIME, Monograph vol. 5 of the Henry L. Doherty series, second printing.

Hantush, M.S., 1966, Analysis of Data from Pumping Tests in Anisotropic Aquifers, Journal of Geophysical Research, 71(2), p. 421-426.

Hillel, D., 1971, Soil and Water: Physical Principles and Processes, Physiological Ecology series, Academic Press, New York, NY.

Hsieh, P.A., and Neuman, S.P., 1985, Field Determination of the Three-Dimensional Hydraulic Conductivity Tensor of Anisotropic Media: 1. Theory, Water Resource Research, Vol. 21, No. 11, Nov. 1985, p. 1655-1665.

Hsieh, P.A., Neuman S.P., Stiles, G.K. and Simpson, E.S., 1985, Field Determination of the Three-Dimensional Hydraulic Conductivity Tensor of Anisotropic Media: 2. Methodology and Application of Fractured Rocks, Water Resource Research, Vol. 21, No. 11, Nov 1985, p. 1667-1676.

Katz, D.L., Cornell, D., Kobayashi, R.L., Poettmann, F.H., Vary, J.A., Eilenbaas, J.R., and Weinaug, C.F., Handbook of Natural Gas Engineering, McGraw-Hill Book Co., Inc., New York, 1959.

Montazer, P., and Wilson, W.E., 1984, Conceptual Hydrologic Model of Flow in the Unsaturated Zone, Yucca Mountain, Nevada, U.S. Geological Survey Water-Resources Investigations Report 84-4345, 55 p.

Muskat, M., 1937, Flow of Homogeneous Fluids Through Porous Media, McGraw-Hill Book Co., New York, 1937.

Papadopoulos, S., Nonsteady flow to a well in an infinite anisotropic aquifer, in Proceedings of the Dubrovnik Symposium on Hydrology of Fracture Rocks, pp. 21-31, International Association of Scientific Hydrology, Debrovnik Yugoslavia, 1965.

Pruess, K., TOUGH User's Guide, Earth Science Division, Lawrence Berkeley Laboratory, University of California, Berkeley, CA, Nov 1985.

Snow, D.T., 1965, A Parallel Model of Fractured Permeable Media, Ph.D. thesis, University of California, Berkeley, CA.

Snow, D.T., 1966, Three-Hole Pressure Test for Anisotropic Foundation Permeability, Felsmech. Ingenieurgeol., 4(4), p. 298-

314.

Rissler, P., 1978, Determination of Water Permeability of Jointed Rock, Publications of the Institute for Foundation Engineering, Soil Mechanics, Rock Mechanics, and Water Way Construction, RWTH (university) Aachen, Federal Republic of Germany, English edition of volume 6, ISSN 0341-7972.

Rowan, G., and Clegg, M.W., Sept. 1982, An Approximate Method for Transient Radial Flow, Society of Petroleum Engineers Journal, p. 225-258.

Van Genuchten, M. Th., 1980, A Closed Form Equation for Predicting the Hydraulic Conductivity of Unsaturated Soils, Soil Scienc Soc. of America Journal, Vol. 44, No. 5, p. 892-898

Van Golf-Racht, T.D., 1982, Fundamentals of Fractured Reservoir Engineering, Developments in Petroleum Science, 12, Elsevier Scientific Publishing Co., New York, NY.

Zimmerman, R., Sandia National Laboratories, 1987 G-Tunnel Underground Facility Tour, handouts and personal communications.

**APPENDIX A**

**CROSS-HOLE PNEUMATIC AND HYDRAULIC PROTOTYPE TEST  
SCHEDULES AND MILESTONES**

Table 2.4-3. Time line task table report

Task Code	Task Description
DAPPROVAL	WMPO technical and QA approval of SIP
DCALIB	Calibration of sensors for Cross-hole field testing
DDTP	Detailed Test Plan writeup for pneumatic & hydraulic cross-hole testing
DDTPM	Completion of DTP for cross-hole testing
DFRPT	Completion of final reports including interpretive and technical documents
DLOG&TVC	Log cross-contact boreholes; TV, neutron probe and fracture logs
DLOG&TVF	Log fault intersection borehole; TV, neutron probe, and fracture logs
DLOG&TVG	Log Bulk Permeability prototype test boreholes; TV, neutron probe, and fracture logs
DMONITORC	Monitor water injection cross-contact test in order to characterize capillary barrier
DMONITORF	Monitor water injection fault test in order to characterize known fault
DMONITORG	Monitor gas injection fracture/matrix test to determine 3-dimensional permeability tensor of Grouse Canyon member
DPO	Prepare purchase orders for equipment
DPROC	Prepare preliminary procedures for testing
DREPORT	Prepare preliminary administrative reports and deliver cross-hole pneumatic & hydraulic test system for use in the ES
DSEQEQUIP	Secure test equipment from vendor
DSIP	Prepare Scientific Investigation Plan (SIP)

TABLE 2.4-3. Time line task table (continued)

Task Code	Task Description
DTESTC	Conduct short term gas injection tests across hydrogeologic contact
DTESTF	Conduct short term gas injection tests along known fault
DTESTG	Conduct fracture location tests in boreholes parallel to axis of proposed Bulk Permeability prototype test room
DUSGSREV	USGS technical and QA review/approval of SIP
DWMPOREV	WMPO technical and QA review/approval of SIP
DWO	Prepare work orders for NTS contractors
UDDRILLC	NTS contractor drills cross-contact boreholes
UDDRILLF	NTS contractor drills fault intersection boreholes
UDDRILLG	NTS contractor drills boreholes parallel to axis of proposed Bulk Permeability prototype test room



2-4-80

at the Court Clerk's Office

Page 2

**APPENDIX B**

**APPLICABLE TECHNICAL PROCEDURES  
CURRENTLY AVAILABLE FOR USE**

Table 2.4-4. Applicable technical procedures.

-----Technical Procedure-----		
Number (NWM-USGS- )	Title	Date
HP-12, R1 (under revision)	Procedures for handling and field testing of the core from unsaturated boreholes	08-14-85
HP-74, R0	Use of the Stabili-Therm miniature batch oven	10-28-85
HP-32, R0	Method for monitoring mois- content of drill-bit cuttings from the unsatu- rated zone	05-15-85
HP-73, R0	Calibration and use of the Sartorius electronic top- loader (balance) Model 1507MPS	03-29-85
HP-55, R0 (to be revised)	Hydrologic-laboratory test- ing of core and drill-cut- ting samples from unsaturated zone test holes	01-16-85
HP-18, R0	Frequency of equipment cali- bration for unsaturated-zone testing, Nevada Test Site	07-24-84
HP-28, R0	Laboratory procedures for the determination of mois- ture-retention curves of rock core	05-16-85
HP-62, R0	Method for measuring mois- ture content using a neutron moisture meter	10-28-85
HP-68, R1 (to be revised)	General procedure for gas sampling from unsaturated zone test hole	(no date)
HP-17, R0	Laboratory procedure for calibration of pressure transducers	08-14-84

Table 2.4-4. Applicable technical procedures (continued)

-----Technical Procedure-----		
Number (NWM-USGS- )	Title	Date
HP-14, RO (under revision)	Laboratory procedure for calibration of thermocouple psychrometers	07-09-84
GP-10, RO	Borehole video fracture logging	04-12-85
GP-11, RO	Logging fractures in core	05-16-85
MDP-01, RO	Identification, handling, storage and disposition of drill-hole core and samples	--

U.S. GEOLOGICAL SURVEY  
WATER RESOURCES DIVISION  
COLORADO WATER  
RESOURCES LIBRARY